Role of the cytosolic domain of occludin in trafficking and HCV infection 1 Running Title: OCLN C-terminus and HCV entry 2

Muriel Lavie, Lydia Linna, Rehab I Moustafa, Sandrine Belouzard, Masayoshi Fukasawa, Jean Dubuisson

Role of the cytosolic domain of occludin in trafficking and HCV infection

Running Title: OCLN C-terminus and HCV entry

Muriel Lavie[1], Lydia Linna[1], Rehab I. Moustafa[1,2], Sandrine Belouzard[1], Masayoshi Fukasawa[3], Jean Dubuisson[1]

[1]Univ. Lille, CNRS, Inserm, CHU Lille, Institut Pasteur de Lille, U1019 - UMR 8204 - CIIL - Center for Infection and Immunity of Lille, F-59000 Lille, France; [2]Department of Microbial Biotechnology, Genetic Engineering and Biotechnology Division, National Research Center, Dokki, Cairo, Egypt; [3]Department of Biochemistry & Cell Biology, National Institute of Infectious Diseases, Tokyo, Japan

Synopsis

The importance of the C-terminal part of OCLN for HCV infection was assessed by a serial deletion approach. The characterization of OCLN mutants revealed that the first 18 residues of the C-terminal cytosolic tail constitute the minimal region required for HCV infection in non-polarized and polarized hepatocyte, despite a loss of TJ localization. Among these 18 residues, I279 and W281 were crucial for cell surface expression of OCLN mutant and modulated its ability to mediate HCV infection.

Abstract

The role of the tight-junction (TJ) protein occludin (OCLN) in hepatitis C virus (HCV) entry remains elusive. Here, we investigated the OCLN C-terminal cytosolic domain in HCV infection. We expressed a series of C-terminal deletion mutants in Huh-7 cells KO for OCLN and characterized their functionality in HCV infection and trafficking. Deleting the OCLN cytosolic domain led to protein instability and intracellular retention. The first 15 residues (OCLN-C15 mutant) of the cytosolic domain were sufficient for OCLN stability, but led to its accumulation in the trans Golgi network (TGN) due to a deficient cell surface export after synthesis. In contrast, OCLN-C18 mutant, containing the first 18 residues of the cytosolic domain, was expressed at the cell surface and could mediate HCV infection. Point mutations in the context of C18 showed that I279 and W281 are crucial residues for cell surface expression of OCLN-C18. However, in the context of full-length OCLN, mutation of these residues only partially affected infection and cell surface localization. Importantly, the characterization of OCLN-C18 in human polarized hepatocytes

revealed a defect in its TJ localization without affecting HCV infection. These data suggest that TJ localization of OCLN is not a prerequisite for HCV infection in polarized hepatocytes.

Acknowledgements

We thank C. Rice and T. Wakita for providing essential reagents. We thank S. Ung for help in assembling figures and Y. Rouillé for his diligent proofreading. The immunofluorescence analyses were performed with the help of the imaging core facility of the BioImaging Center Lille Nord-de-France. Rehab I. Moustafa was supported by a fellowship from the Egyptian Government.

Keywords

Hepatitis C virus, virus entry, virus-host interaction, occludin, tight junctions, trafficking

Introduction

With 70 million people infected, hepatitis C virus is a major health burden. In most cases, HCV establishes chronic infection that eventually leads to the development of cirrhosis and hepatocellular carcinoma (HCC). This positive single-stranded RNA virus infects almost exclusively human hepatocytes. Restriction of HCV infection to hepatocytes is partially due to the specific entry of the virus into these cells. Several lines of evidence show that HCV entry into cells is a complex multistep process that involves a series of specific cellular entry factors. Among them, scavenger receptor BI (SR-BI), tetraspanin CD81 and tight-junction (TJ) proteins claudin-1 (CLDN1) and occludin (OCLN) constitute the four major factors essential for HCV entry [1-3]. SR-BI and CD81 have been shown to interact with the E2 HCV envelope protein and their role in HCV entry has been well documented. On the contrary, no direct interaction between HCV envelope proteins and the TJ proteins CLDN1 and OCLN was reported. CLDN1 contributes to a post-binding step of HCV entry by interacting with CD81 thus facilitating virus internalization [4,5].

OCLN seems to play a role at a late entry step. However, its precise role in the HCV life cycle remains poorly understood. Noteworthy, CD81 and OCLN determine the tropism of HCV for human cells. Since CLDN1 and OCLN are TJ proteins, it was initially thought that HCV virions would migrate to TJs for internalization; however, experimental data could not support this hypothesis until recently [5-10]. Indeed, imaging of HCV entry in a three-dimensional polarized hepatoma system revealed a sequential engagement of the entry factors with an initial localization of HCV with SR-BI and CD81 at the basolateral membrane and a subsequent accumulation of the virus at the TJs in an actin-dependent manner [11].

TJs are specialized sites of cell-cell contacts involved in signalling and formation of the paracellular barrier between epithelial cells and endothelial cells. OCLN was the first integral membrane protein to be identified at TJs. Its tetraspan topology orients two loops in the extracellular space (EC1 and EC2) with the N- and C-termini within the cell [12]. OCLN functions at TJs are poorly understood. It is involved in the regulation of paracellular permeability and cell adhesiveness. The 4 transmembrane segments of OCLN constitute the MARVEL (MAL and related proteins for vesicle trafficking and membrane link) domain that is common to two additional junctional

proteins (tricellulin and MARVEL-D3) and is involved in membrane apposition [13]. The extended (259aa) C-terminal cytosolic domain is endowed with signaling functions. It mediates interaction with scaffolding proteins and subcellular trafficking of the protein and is subjected to numerous post-translational modifications, suggesting it has an important functional role [12,14]. In this context, we sought to determine the role of the OCLN C-terminal cytosolic domain during HCV infection. For this purpose, we expressed a series of C-terminal deletion and point mutants in Huh-7 cells KO for OCLN and characterized their functionality towards HCV infection and cellular trafficking.

Our data showed that deletion of the OCLN cytosolic domain leads to protein instability and intracellular retention. The first 15 residues of the cytosolic domain (C15, aa281-522 deleted) were sufficient to restore protein stability but not cell surface export nor HCV infection. Moreover, OCLN-C15 was retained in the trans Golgi network (TGN) most probably due to a defect in the transport of the protein to the cell surface after its biosynthesis. In contrast, the first 18 residues of the cytosolic domain (C18, aa284-522 deleted) led to cell surface expression and HCV infection. Among these residues I279 and W281 were crucial for the cell surface export of OCLN-C18 and its ability to mediate infection. In OCLN full-length background, mutation of I279 and W281 modulated HCV infectivity with no striking effect on its subcellular localization. Finally, in polarized hepatocytes, OCLN-C18 did not localize at TJs but was still functional for infection.

Results

The first 18 cytosolic residues of the OCLN C-terminal tail are important for HCV infection and OCLN cell surface localization

In order to determine the potential role of the cytosolic C-terminal tail of OCLN in HCV infection, we generated a series of C-terminal deletion mutants. The first deletion corresponded to the removal of the C-terminal distal domain that contains 3 α-helices (aa416-522) involved in interactions with partner proteins [15,16]. We also generated 10 additional mutants by serially deleting 15 C-terminal residues per construct (Figure 1). The different OCLN mutants carried an N-terminal HA epitope

tag and were cloned in the pTRIP lentiviral expression plasmid. A Huh-7-derived cell clone knockout for OCLN (OKH4 cells) [17] was used to characterize the ability of the different constructs to mediate HCVcc entry. OKH4 cells were transfected with the different constructs and infected with HCVcc virus at 48h post-transfection. Infectivity levels were determined at 30-32h post-infection by immunofluorescence using an antibody directed against the E1 viral protein. Expression levels of the mutants were analyzed at the time of infection by Western blotting (Figure 2A). For most of the deletion mutants, besides the band of predicted size, we could also detect a second band migrating closely to the major band that could correspond to the mono-ubiquitinated form of the corresponding protein. In agreement with this hypothesis, several lysines of the C-terminus part of OCLN (K276, K283, K299) have been reported to be ubiquitinated in 293T cells [18]. However, we failed to detect the presence of ubiquitin by Western blotting after precipitation of HA-tagged OCLN (data not shown). Alternatively, these secondary products could correspond to truncated forms of OCLN as proposed previously by Liu *et al.* or to an uncharacterized post-translational modification [19]. As expected, the expression of an OCLN mutant lacking the second extracellular loop (ΔEC2) did not allow HCVcc to infect OKH4 cells, whereas the complementation of OKH4 cells with the full length OCLN protein led to the infection of OKH4 cells by HCVcc (Figure 2B). Surprisingly, most of the deletion mutants were functional for HCVcc infection reaching levels of infectivity ranging from 50% up to 100% of the level obtained with wild-type OCLN. Interestingly, OCLN lacking the entire cytosolic domain failed to complement OKH4 cells for HCV infection. Moreover, this construct accumulated at lower level in the cells as shown by the Western blot analysis. This result suggests that the C-terminal cytosolic tail of OCLN is important for the stability of the protein. While OCLN mutant harboring the first 15 cytosolic residues after the last transmembrane segment (C15, aa281-522 deletion) accumulated at the same level as wild-type OCLN in OKH4 after transfection, this truncated protein did not confer susceptibility to HCVcc infection in OKH4. In contrast, the complementation with OCLN mutant harboring the first 30 cytosolic residues of the C-terminal tail (C30, aa296-522 deletion) restored HCV infection, indicating that important residues for HCV infection were located between residues 281 and 296 of OCLN C-terminal cytosolic domain. To further identify the functional residues located in this region, four additional deletion mutants carrying shorter deletions at aa284-522 (C18), aa287-522 (C21), aa290-522 (C24), aa293-

522 (C27) were generated (Figure 2C, 2D). It is worth noting that the C18 mutant that contains three additional residues downstream of the OCLN-C15 C-terminal sequence was able to restore HCV infection suggesting that residues 281, 282, 283 constituted or were part of a crucial motif for OCLN to mediate HCV entry.

OCLN mutant C15 accumulates in the TGN compartment

The C-terminal tail of OCLN is known to be important for OCLN subcellular localization [20,21]. Thus, the lack of infection observed for the C15 mutant could be due to a defect in cell surface localization of this protein. To test this hypothesis, we analyzed the cell surface expression of OCLN mutants in a biotinylation assay (Figure 3A). We used sulfo-NHS-SS-biotin to specifically label plasma membrane bound HA-tagged OCLN constructs. Biotinylated cell surface proteins were subsequently precipitated with streptavidin-conjugated agarose beads. OCLN present at the cell surface was then analyzed by Western blotting using an anti-HA antibody. Whereas similar levels of biotinylated OCLN could be detected for wild-type OCLN and OCLN-C18, a weaker signal (corresponding to 24% of the intensity of wild-type OCLN) was obtained for OCLN-C15 showing that this mutant was less efficiently exported to the cell surface.

To further characterize the subcellular localization of OCLN-C15 mutant, transfected cells were processed for immunofluorescence detection of HA-labeled wild-type and mutant OCLN (Figure 3B). Whereas wild-type OCLN and OCLN-C18 were mainly observed at the plasma membrane of OKH4 cells, OCLN-C15 and OCLNΔC accumulated intracellularly. Altogether, these results suggested that the first 18 residues (aa266 to 283) of the C-terminal tail of OCLN are required for OCLN cell surface localization.

The analysis of OCLN-C15 mutant subcellular localization by confocal microscopy revealed a perinuclear staining, suggesting an endoplasmic reticulum (ER) or a trans Golgi network (TGN) localization of the protein in transfected OKH4 cells. To further characterize the subcellular localization of this mutant, we performed colocalization experiments using different subcellular compartment markers. As shown in Figure 4A, OCLN-C15 colocalized with the TGN marker, TGN46 with a Pearson correlation coefficient value of 0.6, indicating a substantial overlap. In contrast, no significant colocalization was observed with the calreticulin (CRT), an ER resident protein (Pearson correlation coefficient: 0.2) (Figure 4B). On the contrary, wild-type OCLN

localized mainly at the plasma membrane and did not overlap with the TGN and ER markers (Pearson correlation coefficient: 0.15 and 0.2 respectively). This result indicates that deletion of the residues 281-522 of the C-terminal cytosolic part of OCLN leads to an accumulation of the protein in the TGN.

Deletion of residues 281-522 of OCLN does not affect the fate of cell surface expressed OCLN

Intracellular accumulation of OCLN-C15 could be due to a defect in the targeting of the protein to the plasma membrane along the secretory pathway or to an impaired recycling to the cell surface after internalization. To distinguish between these two hypotheses, we characterized the trafficking of the fraction of OCLN-C15 that reached the cell surface using a biotinylation assay (Figure 5). In a first step, we evaluated the ability of the protein to internalize at 37°C. For this purpose, cell surface proteins were biotinylated at 4°C and the cells were subsequently incubated at 37°C for different periods of time, allowing their internalization. Thereafter, the biotin that remained at the cell surface was cleaved. This way, biotinylated proteins corresponded to internalized proteins. Biotinylated proteins were then precipitated with streptavidin-agarose beads and OCLN detected by Western blotting. As a control experiment, we monitored the endocytosis of the transferrin receptor whose cellular trafficking is well documented (Figure 5C). As shown in Figure 5, similar fractions of cell surface wild-type OCLN (Figure 5A) and OCLN-C15 (Figure 5B) internalized with close kinetics (Figure 5D).

A fraction of OCLN has been previously shown to recycle back to the plasma membrane [22]. Since OCLN-C15 was able to internalize, we tested its ability to recycle back to the plasma membrane. To do so, cell surface proteins were biotinylated and cells incubated at 37°C to induce their internalization. After this step, cell surface biotin was removed by cleavage, which resulted in a selective biotinylation of internalized proteins. A second step of incubation at 37°C during different periods of time allowed internalized protein to potentially recycle back to the plasma membrane. For each time point, one sample was then treated with reduced glutathione to remove the biotin from the proteins that recycled back to the cell surface (internalized biotinylated proteins, Figure 6 biotin cleavage +), whereas another sample was left untreated (total biotinylated proteins, Figure 6 biotin cleavage -). In this experimental setting, the amount of OCLN proteins that recycled to the cell surface corresponds to

the difference between untreated and treated samples. Calculation of the recycling rate for wild-type OCLN and OCLN-C15 did not reveal any significant difference between these two proteins (Figure 6A and 6B). In both cases, the proportion of recycled OCLN reached a maximum of 25% (Figure 6D), whereas 90% of the TfR was found to recycle back to the cell surface in the same conditions (Figure 6C and D). This result is in agreement with a previous report showing that 20% of internalized OCLN is transported back to the cell surface [22]. Altogether these findings did not show major differences between OCLN-C15 mutant and wild-type OCLN for their trafficking in the endocytic pathway after their internalization from the plasma membrane.

To further confirm that the accumulation of OCLN-C15 in the TGN was not due to a defect of trafficking of OCLN-C15 in the endocytic pathway, we performed antibody uptake experiments. This approach requires antibodies recognizing the extracellular region of the protein. To our knowledge all currently commercially available OCLN-specific antibodies recognize intracellular epitopes of the protein. To overcome this limitation, we introduced a Flag epitope in the second extracellular loop (EC2) of OCLN at a position (between I212 and Y213) that was previously reported to be neutral for HCV infection [23]. As expected, the introduction of a Flag epitope in wild-type OCLN and OCLN-C15 EC2 did not affect HCV infectivity levels obtained in transfected OKH4 cells (data not shown). 48 hours after transfection of Flag-tagged wild-type OCLN and OCLN-C15 constructs, OKH4 cells were incubated with anti-Flag antibodies for 30 min to label endocytosed OCLN. The cells were then fixed and processed for immunofluorescent detection of anti-Flag antibody. As shown in Figure 7, intracellular staining was observed for wild-type OCLN and OCLN-C15, which corresponds to the detection of the internalized OCLN. In order to further characterize the intracellular trafficking of the internalized OCLN constructs, we performed colocalization studies using markers of the TGN (TGN46), of the recycling endosomes (transferrin receptor) and of the lysosomes/ late endosomes (Lamp1). Although we had previously observed an accumulation of OCLN-C15 in the TGN of transfected cells, no significant colocalization of internalized OCLN with the TGN marker was observed (Figure 7A and D). On the contrary, endocytosed OCLN predominantly colocalized with the TfR receptor (Figure 7B and D). No significant colocalization was observed with the lysosomal marker, Lamp1 (Figure 7C and D). Moreover, OCLN-C15 and wild-type OCLN exhibited the same staining pattern in all

co-labelling immunofluorescence experiments, confirming that the deletion carried by OCLN-C15 had no impact on the OCLN endocytic pathway.

Collectively, these findings indicate that OCLN-C15 accumulation in the TGN does not result from an alteration of trafficking in the endocytic pathway. Consequently, they indicate that it is due to a defect of transport of the newly synthesized protein from the TGN to the cell surface in the secretory pathway.

Identification of the residues involved in the targeting of OCLN to the cell surface

Whereas OCLN-C15 mutant was affected in its ability to reach the cell surface, addition of the next three residues downstream C15 cytosolic region in the OCLN C-terminal cytosolic sequence restored OCLN cell surface expression and as a consequence HCV entry. This suggested that these three residues (W281, D282, K283) were part of a crucial motif for OCLN export to the cell surface. In order to identify residues that are important for OCLN cell surface expression, we created point mutations in the context of OCLN-C18 mutant sequence background. Interestingly, the C-terminal sequence of OCLN-C18 contains an Isoleucine-Leucine sequence that could function as a di-leucine motif. Di-leucine motifs have been shown to constitute Golgi sorting as well as internalization signals [24]. Moreover, OCLN-C18 C-terminal sequence contains an aspartic acid (D275) that could constitute, together with the isoleucine (I279) and leucine (L280) residues, an internalization signal (Figure 8A).

We thus mutated the C-terminal residues of OCLN-C18 starting from D275. Indeed, D275, K276, S277, N278, I279, L280, W281, D282 and K283 were individually replaced by an alanine residue in OCLN-C18 background and cloned in the pTRIP lentiviral vector. After having checked that all the constructs were expressed at similar levels in transfected OKH4 cells (Figure 8B), we evaluated their ability to complement OKH4 cells for HCV infection (Figure 8C). Interestingly, the mutation of residues I279 and W281 led to a 70% decrease of infectivity while for L280A and D282A mutants, a decrease of infectivity of 35% was observed. Unexpectedly, mutation K283A led to an increase of infectivity (Figure 8C). The remaining mutations had no major impact on HCV infection levels. Cumulative mutations of I279 and W281 (IW mutant) and I279 L280 W281 and D282 (ILWD mutant) did not result in any decrease of infectivity compared to that observed for the single I279A and

W281A mutants suggesting that these residues were concomitantly required for OCLN-C18 functionality (Figure 8C). We then tested the importance of these residues in the context of full-length OCLN. As shown in Figure 8C, single mutations in the I279 or W281 residues led to a decrease of infection of approximately 50%, in the full-length OCLN background. As observed for the OCLN-C18 mutants, the cumulative IW and ILWD mutations did not significantly increase the deleterious effect of individual mutations on HCV infection (Figure 8C). Together, these results show that I279 and W281 constitute key residues for HCV infection in the context of OCLN-C18 and modulate the ability of full-length OCLN to mediate infection.

As observed for OCLN-C15 mutant, the effect of IW mutations on HCV infection could be the consequence of a defect in cell surface expression of OCLN. Moreover, the weaker effect of IW and ILWD mutations on the ability of full-length OCLN to mediate HCV infection could be due to the presence of additional cell surface export signal or sequences compensating the function of IW during infection in the C-terminal part of the protein. To test this hypothesis, we introduced IW and ILWD mutations in OCLN C-75 and OCLN-150 mutants that harbour shorter deletion of the C-terminal tail than OCLN-C18 mutant (Figure 8D). Noteworthy, OCLN C-terminus contains a tyrosine-based motif at position 481-484 (YNRL) and a site (FYXXXXY residues 336-342) potentially involved in caveolar endocytosis [14,25,26]. To determine whether these motifs contributed to the ability of the IW and ILWD full-length OCLN mutants to mediate infection, we cumulated I279A and W281A mutations with that of residues F336, Y337, Y342, Y481 and L484 in the OCLN-TYR-IW mutant. OCLN-TYR mutant that only contained mutations of the potential tyrosine based motifs as well as OCLN-C150 mutant were fully competent for HCV infection in OKH4 cells (Figure 8D). As observed in the context of full-length OCLN, introduction of I279A and W281A mutations in OCLN-C150 and OCLN-TYR mutants led to a 30 to 40% decrease of the infectivity levels obtained for wild-type OCLN in OKH4 cells. OCLN-C75 mutant was associated with a 30% decrease of the infectivity level and introduction of IW mutations in that mutant further impacted its ability to mediate infection by 13% (corresponding to a residual infectivity of 50 %). As observed in full-length OCLN, no significant differences of phenotypes were observed when IW or ILWD residues were mutated in the different OCLN mutants' context (data not shown). The weak impact of IW mutations in OCLN-C150, OCLN-TYR and OCLN-

C75 mutant backgrounds suggests that these mutants still contain signals compensating the absence of I279 and W281 residues for HCV infection.

We then sought to determine if, as found for OCLN-C15, the decreased ability of the OCLN C18I, C18L, C18W, C18D, C18IW, C18ILWD, OCLN_IW, and OCLN_ILWD mutants to mediate infection was correlated to a defect in cell surface expression. For this purpose, we performed cell surface protein biotinylation experiments. While similar levels of HA-tagged wild-type and OCLN mutants were observed in the lysates (Figure 9A), significant differences in the amounts of biotinylated wild-type and mutant OCLN were observed. Thus, as for OCLN-C15, weaker signals were observed for the OCLN-C18I, C18W, C18IW, and C18ILWD mutants, compared to wild-type OCLN and OCLN-C18 (Figure 9A). This result shows that the OCLN C18I, C18W, C18IW, and C18ILWD mutants are less efficiently exported to the cell surface. Conversely, the C18L and C18D mutants were not affected in their cell surface expression, which is in agreement with the weaker impact of these mutations on HCV infection. Furthermore, no significant differences in the amount of biotinylated OCLN were observed for the OCLN_IW and OCLN_ILWD mutants, indicating that these mutations have no major impact on the cell surface expression in the context of the full-length OCLN.

Next, we tested the effect of the mutations on the subcellular localization of OCLN. In agreement with the strong effect of I279A and W281A mutations on the ability of OCLN-C18 to mediate HCV infection, we observed an intracellular accumulation of both mutants as described for the OCLN-C15 mutant. The results of OCLN co-labeling with TGN46-specific antibody in immunofluorescence experiments indicated that similarly to what was observed for OCLN-C15, the mutants C18I and C18W were mainly localized in the TGN (Figure 9 B and C).

In contrast, confocal microscopy analysis of the subcellular localization of the OCLN_IW, OCLN_ILWD, OCL-C75, OCLN-C75IW, OCLN-C150IW and OCLN-TYR-IW mutants did not show any significant change in the protein localization as compared to the wild-type OCLN protein. Indeed, in all cases, the proteins were detected at the plasma membrane (Figure 9B and C and Supplementary Figure 1). This result is in line with the weaker effect observed for these mutants regarding HCV infection (Figure 8C and 8D).

Mutation of I279 and W281 in the context of full-length OCLN affected HCV infection with no significant effect on the cell surface expression of the protein (Figure 8C and

9). Since I279 and L280 residues could potentially constitute an internalization signal, the decrease in infectivity observed for OCLN_IW mutant could be due to a defect in the internalization of the protein. To test this hypothesis, we performed internalization assays after cell surface biotinylation. As shown in Figure 10, no significant difference between the internalization kinetics of wild-type OCLN and OCLN_IW could be observed, excluding any effect of the mutations on OCLN internalization.

N-linked carbohydrates can restore cell surface transport of TGN-retained OCLN mutants

N-glycans have been shown to constitute apical sorting signals [27] and to promote cell surface expression of membrane proteins deleted from their basolateral sorting signals in non-polarized cells [28]. Thus, Gut and collaborators have shown that the addition of N-glycosylation sites in the extracellular loops of OCLN deleted from its C-terminal cytosolic domain allowed the restoration of the cell surface expression of the protein in CHO cells [28]. In a similar manner, we tested the effect of the insertion of N-glycosylation sites in the extracellular loops of OCLN deletion mutants that exhibited a TGN intracellular retention. As previously reported in Gut *et al.* 1998, the introduction of N-glycosylation sites in OCLN-C18 resulted in a shift of the bands corresponding to the OCLN protein in anti-HA Western blotting (Figure 11A). Several bands of different molecular weights could be detected for the C15 and C18IW mutants that could represent high mannose and complex glycosylated forms of the protein. Treatment of the transfected OKH4 cell lysates with the PNGase F amidase, which cleaves between the innermost GlcNAc and asparagine residues of high mannose, hybrid and complex oligosaccharides, led to the recovery of the non-glycosylated OCLN proteins (Figure 11A). Interestingly, the addition of N-glycoslylation sites in the OCLN sequence restored the cell surface expression of OCLN-C15 and C18IW mutants in OKH4 cells (Figure 11B). However, despite the recovery of the cell surface expression of these OCLN mutants, the insertion of N-glycosylation sites did not restore the functionality of these mutants towards HCV infection (data not shown). This result might be due to the masking of OCLN regions involved in HCV infection by the N-glycans. We thus tested the effect of the addition of a single N-glycosylation site in the first extracellular loop (EC1) of OCLN. This modification was sufficient to restore the cell surface expression of the C15 and C18IW mutants but did not allow the protein to mediate HCV infection (data not

shown). However, again, we cannot exclude that the presence of this glycan interferes with the role of OCLN during HCV infection. In agreement with this hypothesis, addition of a N-glycolysation site in EC1 of wild-type OCLN and OCLN-C18 compromised the ability of the proteins to mediate HCV infection (data not shown).

Impact of C-terminal mutations on the addressing of OCLN to the tight junctions and on HCV infection in polarized Huh-7 cells

Our data show that the deletion of the OCLN C-terminus from aa284 to aa522 (C18 mutant) has no impact on the cell surface expression of OCLN and on its role during HCV infection. However, the deletion of the C-terminal domain might potentially affect its ability to associate with TJs and modulate their functions. In order to determine the functionality of the different OCLN mutants in a more physiologically relevant system, we used polarized Huh-7 derived cells [9]. Thus, Huh-7 clone 1sc3 cells that polarize in the presence of DMSO were transduced by lentiviral vectors expressing wild-type or mutants OCLN. At two days post-transduction, the localization of the different mutants and wild-type OCLN was determined by immunofluorescence. In parallel, the TJ protein ZO1 was labeled to control the polarization level of the cells. As expected, we observed a colocalization of wild-type OCLN and ZO1 in the area of cell-to-cell contact suggesting a targeting of OCLN at the TJs in Huh-7 clone 1sc3 cells (Figure 12A, B and C). Whereas a labeling pattern similar to that of wild-type OCLN was observed for the OCLN_IW, C15 and C18IW mutants accumulated intracellularly in a similar manner to what was observed in transfected OKH4 cells. Surprisingly, OCLN-C18 mutant that was expressed at the cell surface of transfected OKH4 cells did not present any colocalization with ZO1 but appeared to be rather scattered at the cell surface of polarized 1sc3 clone cells. This result suggests that the deletion of the 284-522 residues leads to a loss of OCLN targeting to TJs in 1sc3 polarized cells.

We then sought to determine if the defect in the addressing of OCLN-C18 to the TJs was affecting its ability to mediate HCV infection. For this purpose, we generated OCLN-knockout 1sc3 cells using the clustered regularly interspaced short palindromic repeat (CRISPR)/CRISPR-associated protein 9 system. As shown in panel A of Figure 13, no expression of OCLN was detected by Western blotting analysis using an anti-OCLN mAb in the OCLN-KO 1sc3 cells, whereas a product of

the expected size could be detected in the parental cells.

In order to test the functionality of OCLN mutants regarding HCV infection, OCLN-KO 1sc3 cells were transduced with lentiviral vectors expressing the different OCLN mutants or the wild-type protein. We first characterized the subcellular localization of wild-type and mutant OCLN in complemented cells (Figure 13 panel B and C). Analysis of the cell surface expression of OCLN mutants by biotinylation assay revealed a decrease in the cell surface expression of C15 and C18IW mutants, whereas similar fractions of OCLN_IW and wild-type OCLN were exported to the cell surface (Figure 13B). For the C18 mutant, we observed an intermediate phenotype with a slightly lower fraction than that of wild-type OCLN reaching the cell surface. These results are in agreement with the immunofluorescence analysis (Figure 13C) that showed similar localization patterns to those previously observed in parental clone 1sc3 cells. Thus, OCLN_IW and wild-type OCLN localized at TJs, whereas C15 and C18IW mutants were retained intracellularly and C18 was partially expressed at the cell surface.

In order to further characterize the subcellular localization of OCLN-C18 mutant, we co-transduced OCLN-KO 1sc3 cells with lentiviral expression vectors for OCLN mutants and with lentiviral expression vectors for CD81 or CLDN1 fused to a fluorescent protein (Green Fluorescent Protein and cerulean respectively). Whereas CLDN1 localizes at TJ, CD81 has been shown to be only present at the basolateral pole of 1sc3 cells [9]. In agreement with the data obtained in ZO-1 co-labeling assay, wild-type OCLN colocalized with CLDN1 in the areas of cell-to-cell contact while OCLN-C15 accumulated in the cytosol. OCLN-C18 mutant labelling did not overlap with CLDN-1, confirming the previously observed loss of TJ association of this mutant (Figure 13 D and E). Interestingly, as shown in Figure 13D and E, OCLN-C18 mutant seemed to distribute to the same cell surface areas as CD81 (z section 1 and 2) with no perfect colocalization of both proteins, suggesting that they belong to different domains of the basolateral membrane.

In a second step, we characterized the susceptibility of complemented OCLN-KO clone 1sc3 cells to HCV infection. For this purpose, cells were infected with HCVcc two days after transduction. Similar levels of expression for wild-type and mutant OCLN were observed in transduced cells at the time of infection (Figure 14A).

Infection levels were determined by immunofluorescence. As shown in Figure 14 (panel B), HCV infection profiles in wild-type and mutant OCLN rescued 1sc3 cells were similar to those found in OKH4 cells. Indeed, C15, C18IW and OCLN_IW mutants were affected in their ability to mediate infection, whereas OCLN-C18 was fully competent for infection. In order to confirm this result in fully polarized cells, transduced clone 1sc3 cells were treated with DMSO to reinforce polarization in transwell dishes. This experimental setting allows the specific infection of cells on their basolateral pole. In this context, the impairment of C15 and C18IW mutants for HCV infection was confirmed and C18 mutant was fully functional for infection (data not shown). However, no significant decrease in infection was observed for OCLN-IW mutant.

Finally, despite its inability to be located at TJs, the OCLN-C18 mutant remains competent for HCV infection in polarized cells. This finding strongly suggests that at least in the polarized clone 1sc3 model, the localization of OCLN to TJs is not absolutely required for HCV entry.

Discussion

The role of OCLN in HCV entry remains poorly understood while the C-terminal part of OCLN has been shown to be a key component for the protein functions. Overall, this study aimed at investigating the role of the OCLN C-terminal cytosolic tail in HCV infection. For this purpose, a series of C-terminal deletion mutants were expressed in Huh-7 cells KO for OCLN and their functionality in HCV infection and trafficking were characterized. This approach revealed that the deletion of the OCLN C-terminal cytosolic domain (ΔC) leads to protein instability and intracellular retention. The first 15 residues (C15) of the cytosolic domain were sufficient for protein stability but not for cell surface expression nor HCV infection. Furthermore, the characterization of the subcellular localization of the C15 mutant revealed an accumulation of the protein in the TGN. In contrast, the first 18 residues (C18) of the C-terminal cytosolic domain led to cell surface expression and HCV infection. Among these amino acids, isoleucine 279 and tryptophan 281 of OCLN-C18 were key residues for both cell surface expression and HCV infection. Moreover, mutation of residues I279 and W281 led to the accumulation of OCLN-C18 in the TGN as found for OCLN-C15. In the context of the full-length OCLN, mutation of these residues partially affected the

ability of OCLN to restore the permissivity of OCLN-KO Huh-7 cells to HCV infection but had no significant effect on the cell surface localization of the protein. Finally, the assessment of OCLN-C18 functionality in polarized human hepatoma-derived cells revealed that despite a defect in TJ targeting, this mutant could mediate HCV infection. This result suggests that OCLN localization at TJs is not required for entry of HCV into polarized hepatocytes.

Deletion of the C-terminal cytosolic tail of OCLN led to a decrease in OCLN stability and to an intracellular retention of the protein. The C-terminal part of OCLN, which represents half of the protein length, has been shown to be the target of extensive post-translational modifications that modulate OCLN function in TJs [12]. Moreover, it has been reported to mediate the interaction with scaffolding proteins and the subcellular trafficking of OCLN [20]. Thus, the C-terminal cytoplasmic domain of OCLN is sufficient to mediate efficient basolateral transport of a reporter protein, indicating that it contains basolateral-targeting determinants [20]. In agreement with our data, deletion of the C-terminal domain of OCLN had been previously shown to lead to the accumulation of the protein in the Golgi complex when expressed in polarized Madin-Darby canine kidney cells (MDCK) as well as in non-polarized Chinese hamster ovary cells (CHO) [28]. However, no effect of the deletion on the stability of OCLN was reported in the study of Gut *et al*. In contradiction with our findings, Liu and collaborators found that a Flag-tagged OCLN deleted of its C-terminal tail (Flag OCLNΔC) could confer susceptibility to retroviral particles pseudotyped with HCV envelope proteins (HCVpp) when this mutant OCLN protein was expressed in 786-O renal carcinoma cells that express low level of OCLN [19]. However, they also observed an intracellular retention of the protein when expressed in 293T cells as a GFP-tagged protein. Furthermore, biotinylation analysis of the cell surface expression of the Flag OCLNΔC construct revealed lower levels of protein expression at the cell surface, in agreement with our findings. The different effects of the OCLN C-terminal tail deletion on HCV infection observed in Liu's study as compared to our work could be due to the fact that two distinct infection systems were used to characterize OCLN deletion mutants. Indeed, Liu and colleagues performed their infection experiments with HCVpp and their OCLN mutants were expressed in 786-O carcinoma renal cells, whereas we used HCVcc virus and Huh-7 hepatoma cells KO for OCLN. Since transfected OCLN has been shown to be able to dimerise with

endogenous OCLN, residual expression of low level of OCLN in 786-O cells might have an impact on the functional characterization of OCLN mutants [20].

Our finding that cells complemented with OCLN-C18 displayed phenotypes that were similar to those of the wild-type protein in non-polarized hepatoma-derived cells was surprising. The C-terminal domain of OCLN is 259 aa long and corresponds to half of the protein length, but the presence of only 18 residues of the C-terminal domain was sufficient to restore the ability to mediate HCV infection, as well as the localization of OCLN at the cell surface. This raised the question of the role of the remaining part of the C-terminal domain. However, the use of polarized hepatoma-derived cells showed the importance of the remaining part of the cytosolic tail of OCLN for its TJ association. Our results are in agreement with the findings showing that the distal C-terminal part of OCLN mediates the interaction of the protein with scaffolding proteins such as ZO1 [15] and is required for the localization of OCLN at the site of cell-to-cell junctions. However, despite its mislocalization, OCLN-C18 could still render OCLN KO polarized hepatoma-derived cells competent for HCV infection. This result suggests that the localization of OCLN to the TJs is not an absolute prerequisite for infection. In line with this hypothesis, a fraction of the CLDN1 pool was found to be expressed together with CD81 and SR-BI at the basolateral membrane of clone 1sc3 polarized cells [9]. Moreover, in this model, HCV entry has been shown to occur preferentially from the basolateral pole of the cell. Thus, the presence of OCLN-C18 at the basolateral membrane would be sufficient to promote HCV infection in polarized cells. Nevertheless, the importance of TJs for HCV infection might depend on the cell culture system used. Indeed, the recent imaging of HCV entry in a three-dimensional polarized hepatoma system revealed an initial colocalization of HCV with basolateral entry factors SR-BI, CD81 and EGFR. This step was followed by an actin-mediated accumulation of the virus at the TJ and its association with OCLN and CLDN1 prior to cell entry [11].

The characterization of the internalization and recycling of the OCLN-C15 mutant did not show any difference with wild-type OCLN. In agreement with the results obtained by Fletcher *et al.* in MDCK cells [22], we found that approximately 20% of internalized OCLN was recycled back to the plasma membrane. This result indicates that the accumulation of the C15 mutant in the TGN is not due to a defect in OCLN recycling but rather to a defect of transport of the protein to the cell surface after its biosynthesis. In agreement with this hypothesis, antibody uptake experiments

performed to characterize the fate of the cell surface expressed C15 mutant did not reveal any difference in the localization of internalized C15 and wild-type OCLN. Indeed, both of them colocalized with the transferrin receptor that follows the fast recycling route from early endosomes as well as the slow recycling route via the endocytic recycling compartment [29].

Our study identified I279 and W281 as crucial residues for the cell surface expression and the functionality in HCV infection of the OCLN-C18 mutant. Moreover, L280 and D282 residues seemed to modulate the function of the protein in HCV infection, most likely in the entry step. The mild effect of L280A and D282A mutations on infection and the absence of effect on cell surface expression suggest that these residues play an indirect role in the trafficking of the protein. Thus, their replacement by alanine induces a local change of the environment of I279 and W281 that might impact their functionality.

As it is the case for the exit from the ER, it is now admitted that linear sorting signals also mediate the targeting of the membrane proteins from the Golgi complex to their assigned membrane compartment [30]. Thus, di-leucine motifs ([DE]XXXL[LI] or DXXLL), tyrosine-based motifs (NPXY or YXXϕ, where X is any amino acid and ϕ is an amino acid with bulky hydrophobic side chain) as well as non-canonical motifs have been shown to be recognized by adaptor protein complexes or adaptor proteins [31] that sort Golgi cargo to different vesicle carriers. In the case of OCLN, a di-leucine motif (D275XXXI279L280) present in the functional OCLN-C18 mutant did not seem to be involved in the trafficking of this mutant since replacing L280 and D275 with alanine had no effect on its cell surface localization. Instead, I279 and W281 residues were crucial for the cell surface export of the OCLN-C18 mutant and their mutation resulted in TGN accumulation of the protein. This result suggested that these residues constitute a TGN export signal in the OCLN-C18 context and further illustrate the diversity of Golgi export signals. While in general the deletion of these signals leads to the apical or non-polarized distribution of the protein, it has also been reported to induce the retention of the protein in the Golgi apparatus in several cases [32,33]. Thus, the mutation of a membrane proximal tribasic motif in the reovirus p14 fusion-associated small transmembrane (FAST) protein was associated with the accumulation of the protein in the TGN [34]. Similarly, the mutation of the Golgi export signals of the potassium channel Kir2.1 that is formed by a patch of residues present

in the tertiary structure of the protein [35] leads to the intracellular accumulation of the protein in the Golgi.

Whereas I279A and W281A mutations clearly affected OCLN-C18 cell surface localization and HCV infection in complemented OKH-4 cells, they only partially affected the functionality of full-length OCLN for HCV infection. Moreover, they had no significant effect on the subcellular localization of the protein or on its internalization. This result suggests that the cytosolic domain of OCLN contains additional independent cell surface export and internalization signals. In agreement with this hypothesis, the OCLN C-terminus contains a tyrosine-based motif at position 481-484 (YNRL) that is associated with clathrin-mediated endocytosis [14,25]. Moreover, it contains a site with high homology with known caveolin-1 binding sequences (FYXXXXY residues 336-342) [26], suggesting that OCLN internalization also involves caveolar endocytosis. However, the OCLN mutant harbouring mutations in these tyrosine-based motifs as well as I279A and W281A mutations was only partially affected in its ability to mediate HCV infection, and no significant effect on the subcellular localization of the protein was observed. These results suggest that these motifs are not crucial for the cell surface expression of OCLN. Alternatively, OCLN trafficking has also been reported to be regulated by post-translational modification of its C-terminal tail [13]. Although the ILWD motif seems to be non-essential to the cell surface localization of the full-length protein, this motif was found to be highly conserved in OCLN among species.

Interestingly, the addition of 2 glycosylation sites in the extracellular loop of the C15 and C18IW mutants restored the cell surface expression of the mutants. Similarly, addition of two N-glycosylation sites in the extracellular loop of the C-terminus deletion mutant of OCLN led to the export of the protein to the apical surface of MDCK cells and the cell surface of non-polarized CHO cells [28]. N-glycans present in the extracytoplasmic domain of proteins have been shown to constitute apical sorting signals [36-38]. The contribution of N-glycans to apical sorting has been shown by the retention of deglycosylated protein at the level of the Golgi complex [28]. The carbohydrate-binding proteins galectins constitute key regulators of cargo molecules bearing N- or O-glycans [39]. Thus galectins 3,4,9 have been implicated in apical sorting in kidney and intestinal cells [40]. Galectins possess multivalent carbohydrate binding sites that allow the clustering of glycoproteins and their associated lipid rafts may participate to the sorting process [41]. However, some galectins may mediate

apical targeting in a lipid rafts independent way [42,43].

Overall, our study allowed the definition of the minimal region of the OCLN C-terminal cytosolic domain required for HCV infection and OCLN cell surface expression. Moreover, it emphasizes the specific involvement of the distal C-terminus domain of OCLN in its TJ association and indicates that OCLN can mediate HCV entry in a TJ-independent manner.

Material and methods

Construction of OCLN mutants

All the OCLN mutants were cloned into the pTRIP vector kindly provided by C. M. Rice (The Rockefeller University, New York, USA). pTRIP vector is a self-inactivating lentiviral vector that express no HIV proteins but instead contains the CMV promoter that controls the expression of cloned genes. The parental pTRIP-OCLN-GFP previously described [44] was modified to generate a construct harboring an N-terminal HA-tagged full-length OCLN. A series of C-terminal OCLN deletion mutants was generated by PCR using pTRIP-OCLN-GFP as template with the forward primer FW-HA-XbaI-OCLN 5'-CCGACTCTAGAGATGTACCCATACGATGTTCCAGAT TACGCTTCATCCAGGCCTCTTGAAAGT-3' containing the HA tag sequence and a series of reverse primers annealing at different positions of the OCLN sequence. For example, the smallest deletion (C150 OCLN Δ416-522) in the cytosolic part of OCLN was obtained using the reverse primer 5'-ATATAGCTCGAGCTAGTCCTCCTCCAGCTC ATCACA-3'. For generation of the 15 residues deletion mutant series, each next reverse primers annealed 45 bases upstream of the 3' end sequence of the downstream primer. PCR products were cloned between the XbaI and XhoI restriction sites of the pTRIP vector.

Point mutants were generated by fusion PCR using forward and reverse overlapping primers containing the codon of the replacement alanine residue.

OCLN ΔEC2 mutant carrying the deletion of aa200-238 was generated as described in [19] and [17] using fusion PCR with FW-XbaI-HA-OCLN and Rev-XhoI-OCLN 5'-ATATAGCTCGAGCTATGTTTTCTGTCTATCATA-3' external primers and FW-ΔEC2

5’- ATGGGAGTGAACCCAGTGGATCCCCAGGAGGCC-3’ and Rev-ΔEC2 5’-CTCCTGGGGATCCACTGGGTTCACTCCCATTAT-3’ internal primers.

For the antibody uptake experiments, a Flag tag was introduced in OCLN EC2 at the F5 position as described in [23]. This was done by fusion PCR using external primers Fw-HA-XbaI-OCLN and Rev-XhoI-OCLN and internal primers Rev-Flag-OCLN 5’-CTTGTCGTCGTCGTCCTTGTAGTCTATTTGTGAACCATATAGAG-3’ and FW-Flag-OCLN 5’- GAC TAC AAG GAC GAC GAC GAC AAG TAT GCC CTC TGC AAC CAA TT-3’ that contains the Flag sequence insert. For introduction of the Flag in the C15 OCLN mutant EC2, the external primer REV-XhoI-C15 5’-ATATAGCTCGAGCTACAAAATATTGGACTTGTCATA-3’ was used.

To replace residues F336, Y337, Y342, Y481 and Y484 of OCLN C-terminus by alanine, the following internal primers were used in fusion PCR: FW-FYY 5’-GACAAGCGGGCAGCACCAGAGTCTTCCGCAAAATCCACG-3’, REV-FYY 5’-CGTGGATTTTGCGGAAGACTCTGGTGCTGCCCGCTTGTC-3’, FW-YNRL 5’-GCTGATGAAGCAAATAGAGCAAAGCAAGTG-3’, REV-YNRL 5’-CACTTGCTTTGCTCTATTTGCTTCATCAGC-3’.

N-glycosylation C15 and C18IW mutants were generated by inserting a N-glycosylation site in EC1 and EC2 as previously described [20]. Briefly, for introduction of a N-glycosylation site in EC1, G119 Y120 G121 residues were replaced by an asparagine-alanine-serine sequon. In EC2, a N-glycosylation site was introduced by replacing the L215 residue by an asparagine and N217 by a serine. These modifications were done by fusion PCR approaches.

Cell culture

HEK293T/17 cells (ATCC), OCLN-knockout human hepatic Hu7.5.1-8-derived OKH4 cells [17], Huh-7.5 [45], Huh-7 [46], Huh-7 clone 1sc3 cells [9] were cultured in Dulbecco’s modified eagle medium (DMEM) (Life Technologies) supplemented with 10% fetal bovine serum, 2mM GlutaMax and non-essential amino acids (Life Technologies).

Antibodies

Mouse anti-HCV E1 mAbs A4 [47] was generated *in vitro* from hybridoma culture using Miniperm apparatus (Heraeus). Rat Anti-HA mAb 3F10 was from Roche, rabbit anti-ZO1 was from Zymed (Life Technologies), mouse anti-tubulin was from Sigma,

sheep anti-TGN46 was from Biorad, rabbit anti-calreticulin was from Stressgen and rat anti-Flag was from Agilent Technologies, mouse anti-Lamp1 was from BD Bioscience, mouse anti-TfR CD71 was from Santa-Cruz, mouse anti-human OCLN mAb (OC-3F10) was purchased from Life Technologies. Secondary antibodies used for immunofluorescence were from Jackson ImmunoResearch.

Virus production

The virus used in this study was based on the JFH1 strain engineered to reconstitute the A4 epitope in E1 [48] with titer-enhancing mutations [49]. Viral RNAs were produced from the plasmid carrying the full-length JFH1 genome by *in vitro* transcription. Viruses were produced by electroporation of viral RNA into Huh-7 cells as previously described [50].

Immunofluorescence

For immunofluorescence microscopy, cells were grown on glass coverslips and fixed with either cold methanol or 3% paraformaldehyde (PFA, Sigma-Aldrich) for 20 min. In the case of PFA fixation, the cells were permeabilized for 3 min in PBS 0.1% Triton X-100. Cells were then incubated in 10% goat serum PBS blocking buffer for 10 min. Both primary and secondary antibody incubations were carried out in blocking buffer for 30 min at room temperature. Nuclei were stained by a 5-min incubation in PBS containing 1 μg/mL DAPI. Coverslips were mounted on glass slides using 4-88 Mowiol-based mounting medium. Images were acquired using an inverted laser scanning confocal microscope (LSM880, Zeiss) using a x63 (1.4 numerical aperture) oil immersion lens. Double-label immunofluorescence signals were sequentially collected by using single fluorescence excitation and acquisition setting to avoid crossover. Images were processed with Image J software. Colocalization was evaluated using the plugin JACoP of ImageJ [51]. The extent of colocalization of HA-OCLN and different subcellular compartment markers was measured with the Pearson's correlation coefficient, which is a correlation coefficient describing the relationship between the intensities in two images.

For the acquisition of Z-stacks of xy sections, 7 to 10 confocal planes separated by 0.4 μm were acquired. The image stacks were processed using Image J.

Western blotting

Cells were rinsed with cold PBS and lysed at 4°C for 20 min in PBS lysis buffer (1% Triton X-100 and mix of protease inhibitors (Roche)). Insoluble material was removed by centrifugation at 4°C. Protein samples were heated for 7 min at 70°C in Laemmli sample buffer and resolved by SDS-PAGE. The proteins were then transferred onto nitrocellulose membranes (Hybond-ECL; Amersham) using a Trans-Blot apparatus (BioRad). Proteins of interest were revealed upon incubation of the membrane with specific primary antibodies followed by incubation with species-specific secondary antibodies conjugated to peroxidase. Detection of proteins was done using enhanced chemiluminescence (ECL Plus, GE Healthcare). Quantification of unsaturated signals was carried out using the gel quantification function of Image J.

Assays based on cell surface biotinylation

Endocytosis

OKH4 cells expressing HA-OCLN constructs were incubated with cleavable EZ-link Sulfo-NHS-SS-Biotin (0.3 mg/mL)(Pierce) in PBS for 30 min at 4°C to label cell surface proteins. Unreacted biotin was quenched with 50 mM glycine in PBS buffer. After washing, cells were incubated at 37°C in DMEM for increasing periods of time. Cells were then rinsed with cold PBS and reduced gluthatione (50 mM) containing buffer (75 mM NaCl, 75 mM NaOH, 10% FBS) to cleave biotin bound to non-endocytosed proteins. Cells were then washed with PBS supplemented with 1% bovine serum albumin and 50mM iodocetamide to quench free SH groups. The cells were then lysed in lysis buffer and biotinylated proteins were recovered using streptavidin-agarose beads (Amersham Biosciences). After washing, the bound proteins were detected by immunoblotting.

Recycling

The procedure used to monitor the recycling of OCLN to the cell surface by a biotinylation approach has been described in detail in Fletcher et al. 2014 [22]. Briefly, cells were labeled with biotin as described above and incubated at 37°C for a 30-min internalization period. This step was followed by removal of biotin from cell surface proteins with reduced glutathione followed by quenching with iodoacetamide, for all except one sample. The non-treated sample and one treated sample were lysed at this stage to quantify the starting pool of internalized OCLN. Then, the remaining samples were incubated a second time at 37°C for increasing periods of time. This

step allowed the restoration of the intracellular trafficking of the proteins. After each time point, one sample was treated with reduced glutathione and quenched, to measure the intracellular biotinylated OCLN pool and a second sample was quenched only, which allowed the measurement of the total biotinylated OCLN pool. Thus, the recycled OCLN pool corresponded to the difference between the total biotinylated OCLN pool and the intracellular biotinylated OCLN pool. Cells were then lysed and lysates were further processed for quantification of biotinylated OCLN as described above.

Endocytosis assay by antibody uptake

HA-OCLN constructs were expressed by transient transfection in OKH4 cells. 48h post-transfection, cells were incubated with rat anti-Flag mAb for 30 min at 37°C. Cells were then rinsed with PBS and fixed with 3% PFA. After permeabilization with PBS 0.1% Triton X-100 the internalized antibody was revealed with either a cy3-conjugated goat anti-rat or an Alexa 488-conjugated donkey anti-rat (Santa Cruz). Subcellular compartment markers were co-labeled using either sheep anti-TGN46, mouse anti-Lamp1 or mouse anti-TfR antibody. Secondary antibodies used were cy3-conjugated donkey anti-sheep or Alexa-488-conjugated goat anti-mouse respectively.

Plasmid transfection

OKH4 cells were seeded in 24-well plates and transfected with 250 ng of plasmid DNA using Trans-IT LT1 transfection reagent (Mirus Bio) according to the manufacturer's instructions. Further analyses were performed at 48h post-transfection.

Lentivirus transduction

pTRIP-CD81-GFP and pTRIP-cerulean-CLDN1 were kindly provided by C. M. Rice (Rockefeller University) [2].

To produce lentivirus stocks, HEK293T/17 cells were seeded in 6-well dishes. The next day, cells were transfected with 500 ng pTRIP vector, 400 ng of HIV gag-pol expressing vector and 100 ng of vesicular stomatitis virus G protein expressing vector with Turbofect (Thermo Fisher) according to the manufacturer's instructions. Virus stocks were collected at 48h post-transfection and filtered.

Clone 1sc3 cells were transduced with lentivirus containing supernatants for 48h before being further analyzed for transgene expression or infected with HCV.

Cell polarization and infection

To increase the level of cell polarization clone 1sc3 Huh-7 cells were seeded on transwell permeable supports (polyester membranes with 3-μm pores; Corning). When cells reached confluency the medium was replaced with William's medium (Life Technologies) supplemented with 10% FBS, 2mM Glutamax, 10 ng/mL gentamycin and 1% DMSO. After 5 days of culture in the presence of DMSO, cells were infected by HCV on the basolateral chamber of the transwell. Cells were lysed at 30h post-infection, and RNAs were extracted with NucleoSpin RNA II kit (Macherey Nagel) according to the manufacturer's instructions. HCV RNA was quantified by quantitative real-time RT PCR assay as described previously [52].

Generation of OCLN-knock out clone 1sc3 Huh-7 cells

To generate OCLN knockout cells, the pSpCas9(BB)-2A-Puro (pX459)(Addgene) was used. Two single-guide RNAs (site A and B) specific for the human OCLN gene described by Shirasago and collaborators [17] were cloned in the pX459 vector. Clone 1sc3 Huh-7 cells were seeded in 6-well plates and transfected with 500 ng of pX459-site A and pX459-site B plasmid using Trans-IT LT1 transfection reagent according to the manufacturer's protocol. Two days post-transfection, the cells having incorporated the plasmids were selected with DMEM containing 2.5 μg/mL puromycin. Four to five days later, the puromycin selection was removed and OCLN knockout was checked by Western blotting.

Acknowledgements

We thank C. Rice and T. Wakita for providing essential reagents. We thank S. Ung for help in assembling figures and Y. Rouillé for his diligent proofreading. The immunofluorescence analyses were performed with the help of the imaging core facility of the BioImaging Center Lille Nord-de-France. Rehab I. Moustafa was supported by a fellowship from the Egyptian Government.

References

1. Dubuisson J, Cosset F-L. Virology and cell biology of the hepatitis C virus life cycle – An update. *J Hepatol*. 2014;61(Supplement):S3–S13. doi:10.1016/j.jhep.2014.06.031.

2. Ploss A, Evans MJ, Gaysinskaya VA, et al. Human occludin is a hepatitis C virus entry factor required for infection of mouse cells. *Nature*. 2009;457(7231):882–886. doi:10.1038/nature07684.

3. Zheng A, Yuan F, Li Y, et al. Claudin-6 and Claudin-9 Function as Additional Coreceptors for Hepatitis C Virus. *J Virol*. 2007;81(22):12465–12471. doi:10.1128/JVI.01457-07.

4. Evans MJ, Hahn von T, Tscherne DM, et al. Claudin-1 is a hepatitis C virus co-receptor required for a late step in entry. *Nature*. 2007;446(7137):801–805. doi:10.1038/nature05654.

5. Harris HJ, Davis C, Mullins JGL, Goodall M, Farquhar MJ, Mee C. Claudin Association with CD81 Defines Hepatitis C Virus Entry. *J Biol Chem*. 2010;285(27):21092–21102.

6. Harris HJ, Farquhar MJ, Mee CJ, et al. CD81 and Claudin 1 Coreceptor Association: Role in Hepatitis C Virus Entry. *J Virol*. 2008;82(10):5007–5020. doi:10.1128/JVI.02286-07.

7. Mee CJ, Grove J, Harris HJ, Hu K, Balfe P, McKeating JA. Effect of Cell Polarization on Hepatitis C Virus Entry. *J Virol*. 2008;82(1):461–470. doi:10.1128/JVI.01894-07.

8. Mee CJ, Harris HJ, Farquhar MJ, et al. Polarization Restricts Hepatitis C Virus Entry into HepG2 Hepatoma Cells. *J Virol*. 2009;83(12):6211–6221. doi:10.1128/JVI.00246-09.

9. Belouzard S, Danneels A, Fénéant L, Séron K, Rouillé Y, Dubuisson J. Entry and release of hepatitis C virus in polarized human hepatocytes. *J Virol*. 2017:JVI.00478–17. doi:10.1128/JVI.00478-17.

10. Coller KE, Berger KL, Heaton NS, Cooper JD, Yoon R, Randall G. RNA interference and single particle tracking analysis of hepatitis C virus endocytosis. *PLoS Pathog*. 2009;5(12):e1000702. doi:10.1371/journal.ppat.1000702.

11. Baktash Y, Madhav A, Coller KE, Randall G. Single Particle Imaging of Polarized Hepatoma Organoids upon Hepatitis C Virus Infection Reveals an Ordered and Sequential Entry Process. *Cell Host Microbe*. 2018;23(3):382–394. doi:10.1016/j.chom.2018.02.005.

12. Dörfel MJ, Huber O. Modulation of Tight Junction Structure and Function by Kinases and Phosphatases Targeting Occludin. *J Biomed Biotechnol*. 2012;2012(3):1–14. doi:10.1074/jbc.M110.186932.

13. Cummins PM. Occludin: One Protein, Many Forms. *Mol Cell Biol*. 2011;32(2):242–250. doi:10.1128/MCB.06029-11.

14. Fletcher SJ, Rappoport JZ. Tight junction regulation through vesicle trafficking: bringing cells together. *Biochem Soc Trans*. 2014;42(1):195–200. doi:10.1042/BST20130162.

15. Li Y, Fanning AS, Anderson JM, Lavie A. Structure of the Conserved Cytoplasmic C-terminal Domain of Occludin: Identification of the ZO-1 Binding Surface. *J Mol Biol*. 2005;352(1):151–164. doi:10.1016/j.jmb.2005.07.017.

16. Furuse M, Itoh M, Hirase T, Nagafuchi A, Yonemura S. Direct association of occludin with ZO-1 and its possible involvement in the localization of occludin at tight junctions. *J Cell Biol*. 1994;127(6):1617–1626. doi:10.1083/jcb.127.6.1617.

17. Shirasago Y, Shimizu Y, Tanida I, et al. Occludin-Knockout Human Hepatic Huh7.5.1-8-Derived Cells Are Completely Resistant to Hepatitis C Virus Infection. *Biol Pharm Bull*. 2016;39:839–848.

18. Wagner SA, Beli P, Weinert BT, et al. A Proteome-wide, Quantitative Survey of In Vivo Ubiquitylation Sites Reveals Widespread Regulatory Roles. *Mol Cell Proteomics*. 2011;10(10):M111.013284. doi:10.1016/j.cell.2005.11.007.

19. Liu S, Kuo W, Yang W, et al. The second extracellular loop dictates Occludin-mediated HCV entry. *Virology*. 2010;407(1):160–170. doi:10.1016/j.virol.2010.08.009.

20. Matter K, Balda MS. Biogenesis of tight junctions: the C-terminal domain of occludin mediates basolateral targeting. *J Cell Sci*. 1998;111:511–519.

21. Mitic LL, Schneeberger EE, Fanning AS, Anderson JM. Connexin-Occludin Chimeras Containing the Zo-Binding Domain of Occludin Localize at Mdck Tight Junctions and Nrk Cell Contacts. *J Cell Biol*. 1999;146(3):683–693. doi:10.1083/jcb.136.2.399.

22. Fletcher SJ, Iqbal M, Jabbari S, Stekel D, Rappoport JZ. Analysis of Occludin Trafficking, Demonstrating Continuous Endocytosis, Degradation, Recycling and Biosynthetic Secretory Trafficking. *PLoS ONE*. 2014;9(11):e111176. doi:10.1371/journal.pone.0111176.s003.

23. Sourisseau M, Michta ML, Zony C, et al. Temporal analysis of hepatitis C virus cell entry with occludin directed blocking antibodies. *PLoS Pathog*. 2013;9(3):e1003244. doi:10.1371/journal.ppat.1003244.g006.

24. Kozik P, Francis RW, Seaman MNJ, Robinson MS. A Screen for Endocytic Motifs. *Traffic*. 2010;11(6):843–855. doi:10.1128/MCB.8.11.4936.

25. Ivanov AI, Nusrat A, Parkos CA. Endocytosis of Epithelial Apical Junctional Proteins by a Clathrin-mediated Pathway into a Unique Storage Compartment. *Mol Biol Cell*. 2004;15:176–188. doi:10.1091/mbc.E03.

26. Itallie CMV, Anderson JM. Caveolin binds independently to claudin-2 and occludin. *Ann NY Acad Sci*. 2012;1257(1):103–107. doi:10.1002/jcp.22590.

27. Rodriguez-Boulan E, Kreitzer G, Müsch A. Organization of vesicular trafficking in epithelia. *Nat Rev Mol Cell Biol*. 2005;6(3):233–247. doi:10.1038/nrm1593.

28. Gut A, Kappeler F, Hyka N, Balda MS, Hauri H-P, Matter K. Carbohydrate-mediated Golgi to cell surface transport and apical targeting of membrane proteins. *EMBO J*. 1998;17(7):1919–1929.

29. Grant BD, Donaldson JG. Pathways and mechanisms of endocytic recycling. *Nat Rev Mol Cell Biol*. 2009;10:597–608. doi:10.1038/nrm2755.

30. Anitei M, Hoflack B. Exit from the trans-Golgi network: from molecules to mechanisms. *Curr Opin Cell Biol*. 2011;23(4):443–451. doi:10.1016/j.ceb.2011.03.013.

31. Bonifacino JS. Adaptor proteins involved in polarized sorting. *J Cell Biol*. 2014;204(1):7–17. doi:10.1074/jbc.274.9.5385.

32. Nishimura N, Balch WE. A Di-Acidic Signal Required for Selective Export from the Endoplasmic Reticulum. *Science*. 1997;277(5325):556–558.

33. Nishimura N, Plutner H, Hahn K, Balch WE. The subunit of AP-3 is required for efficienttransport of VSV-G from the trans-Golginetwork to the cell surface. *Proc Natl Acad Sci USA*. 2002;99(10):6755–6760.

34. Parmar HB, Barry C, Kai F, Duncan R. Golgi complex-plasma membrane trafficking directed by an autonomous, tribasic Golgi export signal. *Mol Biol Cell*. 2014;25(6):866–878. doi:10.1016/j.bbamem.2010.06.015.

35. Ma D, Taneja TK, Hagen BM, et al. Golgi Export of the Kir2.1 Channel Is Driven by a Trafficking Signal Located within Its Tertiary Structure. *Cell*. 2011;145(7):1102–1115. doi:10.1016/j.cell.2011.06.007.

36. Scheiffele P, Peränen J, Simons K. N-glycans as apical sorting signals in epithelial cells. *Nature*. 1995;378:96–98.

37. Yeaman C, Gall AHL, Baldwin AN, Monlauzeur L, Bivic AL, Rodriguez-Boulan E. The O-glycosylated Stalk Domain Is Required for Apical Sorting of Neurotrophin Receptors in Polarized MDCK Cells. *J Cell Biol*. 1997;139(4):929–940. doi:10.1074/jbc.270.30.17815.

38. Alfalah M, Jacob R, Preuss U, Zimmer K-P, Naim H, Naim HY. O-linked glycans mediate apical sorting of human intestinal sucrase-isomaltase through association with lipid rafts. *Current Biol*. 1999;9:593–596.

39. Guo Y, Sirkis DW, Schekman R. Protein Sorting at the trans-Golgi Network. *Annu Rev Cell Dev Biol*. 2014;30(1):169–206. doi:10.1146/annurev-cellbio-100913-013012.

40. Delacour D, Koch A, Jacob R. The Role of Galectins in Protein Trafficking.

Traffic. 2009;10(10):1405–1413. doi:10.4049/jimmunol.176.2.778.

41. Brewer FC. Thermodynamic binding studies of galectin-1, -3 and -7. *Glycoconj J*. 2004;(19):459–465.

42. Delacour D, Cramm-Behrens CI, Drobecq H, Le Bivic A, Naim HY, Jacob R. Requirement for Galectin-3 in Apical Protein Sorting. *Current Biol*. 2006;16(4):408–414. doi:10.1016/j.cub.2005.12.046.

43. Delacour D, Greb C, Koch A, et al. Apical Sorting by Galectin-3-Dependent Glycoprotein Clustering. *Traffic*. 2007;8(4):379–388. doi:10.1083/jcb.200507116.

44. Fénéant L, Ghosn J, Fouquet B, et al. Claudin-6 and Occludin Natural Variants Found in a Patient Highly Exposed but Not Infected with Hepatitis C Virus (HCV) Do Not Confer HCV Resistance In Vitro. *PLoS ONE*. 2015;10(11):1–20. doi:10.1371/journal.pone.0142539.g007.

45. Lindenbach BD, Evans MJ, Syder AJ, et al. Complete replication of hepatitis C virus in cell culture. *Science*. 2005;309(5734):623–626. doi:10.1126/science.1114016.

46. Nakabayashi H, Taketa K, Miyano K, Yamane T. Growth of human hepatoma cell lines with differentiated functions in chemically defined medium. *Cancer Res*. 1982;(42):3858–3863.

47. Dubuisson J, Hsu H, Cheung RC, Greenberg HB, Russel DG, Rice CM. Formation and Intracellular Localization of Hepatitis C Virus Envelope Glycoprotein Complexes Expressed by Recombinant Vaccinia and Sindbis Viruses. *J Virol*. 1994;68(10):6147–6160.

48. Goueslain L, Alsaleh K, Horellou P, et al. Identification of GBF1 as a cellular factor required for hepatitis C virus RNA replication. *J Virol*. 2010;84(2):773–787. doi:10.1128/JVI.01190-09.

49. Delgrange D, Pillez A, Castelain S, et al. Robust production of infectious viral particles in Huh-7 cells by introducing mutations in hepatitis C virus structural proteins. *J Gen Virol*. 2007;88(9):2495–2503. doi:10.1099/vir.0.82872-0.

50. Zhong J, Gastaminza P, Cheng G, et al. Robust hepatitis C virus infection in vitro. *Proc Natl Acad Sci USA*. 2005;102(26):9294–9299. doi:10.1016/j.tibtech.2004.06.002.

51. Harris HJ, Farquhar MJ, Mee CJ, et al. CD81 and Claudin 1 Coreceptor Association: Role in Hepatitis C Virus Entry. *J Virol*. 2008;82(10):5007–5020. doi:10.1128/JVI.02286-07.

52. Castelain S, Descamps V, Thibault V, et al. TaqMan amplification system with an internal positive control for HCV RNA quantitation. *J Clin Virol*. 2004;31(18):227–234. doi:10.1016/j.jcv.2004.03.009.

Figure Legends

Figure 1: Schematic description of the series of C-terminal OCLN deletion mutants. The first deletion corresponds to the removal of the C-terminal distal domain that contains 3 α-helices (aa416-522) involved in interactions with partner proteins (C150 Δ416-522 deletion). Ten additional mutants were generated by serially deleting 15 more C-terminal residues per constructs. The shortest construct carries the deletion of the complete C-terminal cytosolic domain (ΔC, Δ266-522 deletion). ΔEC2 mutant was generated by deletion of residues 200 to 238 of the second extracellular loop. The different mutants are designed by C followed by the number of cytosolic residues present downstream the fourth transmembrane domain of OCLN. The different OCLN mutants carry a N-terminal HA epitope tag and are cloned in the pTRIP lentiviral expression plasmid. A second set of 4 mutants (C18, C21, C24, C27) was generated by removing 3 residues per construct starting from the C30 mutant sequence. Transmembrane domains are represented in red, extracellular loops in blue, intracellular loop in green and cytosolic tails in violet. The distal coiled-coil of OCLN that contains three alpha-helices [1-3] is shown in yellow. The dotted line stands for the non-represented intermediate deletion mutants.

Figure 2: Characterization of OCLN C-terminal deletion mutants.
OKH4 cells were transiently transfected with plasmids encoding the different HA-tagged OCLN deletion mutants and wild-type OCLN (wt), or left untransfected (NT) and infected at 48h post-transfection with HCVcc virus. Expression levels of the mutants after transfection were analyzed at the time of infection by Western blotting using an anti-HA mAb. The equivalent loading of cell lysates was confirmed with an anti-β-tubulin antibody. The positions of the molecular weight ladder (kDa) are shown on the left side of the Western blots (A and C). Infectivity levels were determined at 30-32h post-infection by immunofluorescence assay using an antibody directed against the E1 viral protein (B and D). Infectivity is expressed as the percentage of the infection level obtained in OKH4 cells expressing wt OCLN. Error bars indicate standard errors of at least three independent experiments (SD). * $P < 0.05$; ** $P<0.01$; ***$P< 0.001$ in the paired t-test.

Figure 3: Cell surface expression of OCLN deletion mutants.

A) Cell surface biotinylation of OCLN mutants. OKH4 cells were transfected with plasmids encoding HA-tagged OCLN deletion mutants (C15, C18) and wild-type OCLN (wt). At 48 hours post-transfection, cell surface proteins were biotinylated at 4°C. HA-tagged proteins from the cell lysates were analyzed by Western blotting with an anti-HA mAb (Total). The biotinylated cell surface expressed proteins were pulled down with streptavidin agarose beads. OCLN abundance in these samples was also determined by Western blot analysis using an anti-HA mAb.
B) Subcellular localization of OCLN mutants. OKH4 cells were transfected with plasmids encoding HA-tagged OCLN deletion mutants (ΔC, C15, C18) and wild-type OCLN (wt). At 48 hours post-transfection, the cells were fixed and processed for immunofluorescence detection of HA-tagged wt and mutant OCLN. HA staining is shown in red and nuclei are shown in blue. Bars, 10 μm.

Figure 4: Characterization of the subcellular localization of the OCLN-C15 mutant. OKH4 cells were transfected with plasmids encoding HA-tagged OCLN-C15 mutant and wild-type OCLN (wt). At 48 hours post-transfection, the cells were fixed and processed for double-label immunofluorescence detection of HA-tagged wt OCLN or C15 mutant and the TGN marker, TGN46 (A) or the ER marker, calreticulin (CRT, B). Pearson correlation coefficients calculated for at least 10 cells in each condition are shown. The error bars represent the SD. * $P < 0.05$ in the Wilcoxon signed-rank test. Bars, 10 μm.

Figure 5: Endocytosis kinetics of wild-type OCLN and OCLN-C15 mutant. OKH4 cells were transfected with plasmids encoding HA-tagged wild-type OCLN (wt, A) or C15 mutant (B). At 48h post-transfection, the cells were biotinylated at 4°C and incubated for increasing periods of time at 37°C to allow internalization. The biotin present on cell surface proteins was then removed with reduced glutathione; thus, only internalized proteins remained biotinylated. After cell lysis, the HA-tagged proteins were analyzed by Western blotting with an anti-HA mAb allowing the quantification of HA-OCLN abundance in the lysates of biotinylated cells (A, B, Total). Internalized biotinylated proteins present in the lysates were pulled down with streptavidin agarose beads. Internalized biotinylated OCLN abundance was determined via Western blot analysis using an anti-HA mAb (A, B, Biotinylated). The kinetic of

internalization of the transferrin receptor (TfR, C) was used as the positive control. The signal intensity obtained in the Western blot (biotinylated blot) was quantified for each time point and expressed as the % of the intensity obtained without cleavage of biotin and 37°C incubation (Ctrl). The averages of the values obtained in three repeats are shown. The error bars represent the standard error of the mean.

Figure 6: Kinetics of cell surface recycling of wild-type OCLN and OCLN-C15 mutant. OKH4 cells were transfected with plasmids encoding HA-tagged wild-type OCLN (wt, A) and C15 mutant (B). At 48h post-transfection, the cells were biotinylated at 4°C and incubated for 30 min at 37°C to allow cell surface protein internalization. Biotin was removed from cell surface proteins with reduced glutathione; thus, only internalized proteins remained biotinylated. Cells were then incubated at 37°C for increasing periods of time, thus allowing the recycling of the internalized biotinylated protein to the cell surface. For each time point, two samples were used. The first sample was treated with reduced glutathione (+) to remove biotin while the second was left untreated (-). This way, the glutathione treated sample allowed the quantification of the amount of intracellular protein, while the non-treated sample gave access to the amount of total biotinylated proteins, which is composed, of the intracellular biotinylated proteins and the cell surface recycled proteins. Thereafter cells were lysed and the HA-tagged proteins were analyzed by Western blotting with an anti-HA mAb allowing the quantification of HA-OCLN abundance in the lysates of biotinylated cells (A, B,Total). Biotinylated proteins present in the lysates were pulled down with streptavidin agarose beads and their abundance was determined via Western blot analysis using an anti-HA mAb (A, B, Biotinylated). As an experimental control, the kinetics of the recycling of the transferrin receptor (TfR, C) was determined in parallel. The percentage of recycled proteins at each time point was determined by subtracting the signal intensity obtained after glutathione treatment (biotin cleavage +: intracellular protein) from the signal obtained for the untreated sample (biotin cleavage -: intracellular + recycled biotinylated protein). The difference was then expressed as a percentage of the signal obtained with no incubation at 37°C and no GSH treatment (0 min -, D).

Figure 7: Subcellular localization of internalized wild-type OCLN and OCLN-C15 mutant. OKH4 cells were transfected with plasmids encoding HA-tagged wild-type

OCLN (wt) or OCLN-C15 mutant carrying a Flag tag in the second extracellular loop of the protein. At 48h post-transfection, cells were incubated for 30 min at 37°C with an anti-Flag mAb. Cells were then fixed with PFA and processed for double-label immunofluorescent detection of internalized mAbs together with different intracellular organelle markers (TGN46, A; TfR, B; Lamp1, C). Pearson correlation coefficients calculated for at least 10 cells of each condition are shown. The error bars represent the SD (D). Bars, 10 μm

Figure 8: A) Schematic representation of OCLN-C15 and OCLN-C18 mutants. The amino acid sequence of the cytosolic C-terminal part of each mutant is indicated below OCLN drawings. Residues differing between the two mutants are shown in red. The residues that have been mutated into alanine are depicted in bold characters.
B) Effect of point mutations on the expression of OCLN-C18 and full-length OCLN in complemented OKH4 cells. OKH4 cells were transfected with plasmids encoding the different HA-tagged OCLN mutants or wild-type (wt) OCLN. At 48h post-transfection, the cells were lysed. Loading of equal amounts of proteins was verified by Western blotting using an anti-β-tubulin antibody. The HA-tagged proteins were analyzed by Western blotting with an anti-HA mAb.
C) Effect of point mutations in OCLN-C18 and full-length OCLN on HCV infection of complemented OKH4 cells.
D) Effect of point mutations in OCLN-C75, OCLN-C150 and OCLN-TYR mutants on HCV infection of complemented OKH4 cells. (C and D) OKH4 cells were transfected with plasmids encoding the different HA-tagged OCLN mutants or wt OCLN. At 48h post-transfection, the cells were infected with HCVcc. At 30h post-infection, infection was quantified via immunofluorescence using the A4 anti-E1 mAb and expressed as the percentage of the infection level obtained in OKH4 cells expressing wt OCLN. Mean values and standard deviations from at least three independent experiments are shown. * $P<0.05$ in the Wilcoxon signed-rank test.

Figure 9: A) Cell surface expression of OCLN-C18 and full-length OCLN point mutants. OKH4 cells were transfected with plasmids encoding the different HA-tagged OCLN mutants, or wild-type OCLN (wt). At 48h post-transfection, the cells were biotinylated at 4°C or left untreated (wt Ctrl) and subsequently lysed. Cell surface biotinylated proteins present in the lysates were pulled down with streptavidin

agarose beads. OCLN abundance was determined by Western blot analysis using an anti-HA mAb (Biotinylated). The total amount of HA-OCLN present in the lysate was determined by Western blotting using an anti-HA mAb (Total). B-C) Characterization of the subcellular localization of OCLN-C18 and full-length OCLN point mutants. B) OKH4 cells were transfected with plasmids encoding the different HA-tagged mutant or wild-type OCLN (wt). At 48h post-transfection, the cells were fixed and processed for double-label immunofluorescence detection of TGN46 and HA-tagged wild-type and mutant OCLN. Bars, 10 μm. C) Pearson correlation coefficients calculated for at least 10 cells of each condition are shown. The error bars represent the SD. * P< 0.05; ** P<0.01; ***P< 0.001 in the Wilcoxon signed-rank test.

Figure 10: Kinetics of internalization of wild-type and OCLN_IW mutant. OKH4 cells were transfected with plasmids encoding HA-tagged wild-type OCLN (wt) or OCLN_IW mutant (OCLN _IW). At 48h post-transfection, the cells were biotinylated at 4°C and incubated for increasing periods of time at 37°C to allow internalization. Then, biotin was removed from cell surface proteins with reduced glutathione; thus, only internalized proteins remained biotinylated. After cell lysis, the HA-tagged proteins were analyzed by Western blotting with an anti-HA mAb allowing the quantification of HA-OCLN abundance of biotinylated cells in the lysates (Total). Internalized biotinylated proteins present in the lysates were pulled down with streptavidin agarose beads. Internalized biotinylated OCLN abundance was then determined via Western blot analysis using an anti-HA mAb (Biotinylated).

Figure 11: Rescuing of cell surface expression of OCLN-C15 and OCLN-C18IW mutants by N-glycosylation. OKH4 cells were transfected with plasmids expressing OCLN-C15 and OCLN-C18IW mutants carrying (NC15 and NC18IW) or not carrying (C15 and C18IW) two glycosylation sites in the extracellular loops of the protein. At 48h post-transfection the cells were either lysed for protein glycosylation analysis (A) or fixed with PFA to determine the subcellular localization of the proteins (B). A) The cell lysates were digested (+) or not (-) with PNGase F amidase which cleaves the glycans from N-glycosylated proteins and the OCLN mutants were analyzed by Western blotting using an anti-HA mAb. B) In parallel, PFA fixed cells were processed for double-label immunofluorescence detection of TGN46 and HA-tagged glycosylated (N-C15, N-C18IW) or non-glycosylated C15 and C18IW OCLN mutants.

Pearson correlation coefficients calculated for at least 10 cells of each condition are shown. The error bars represent the SD. * P< 0.05 in the Wilcoxon signed rank test. Bars, 10 μm.

Figure 12: Subcellular localization of OCLN mutants in polarized clone 1sc3 cells. A) Clone 1sc3 cells were transduced with lentiviral vectors to express wild-type OCLN (wt) or the different mutants. At 48h post transduction, cells were fixed and processed for double label staining of ZO1 and HA-tagged wt and mutant OCLN. Nuclei were stained with DAPI. z stacks of xy sections of the cells were acquired by confocal microscopy and three different z sections are presented. Bars, 10 μm. B) Schema showing the relative position of the shown sections.. C) y-z projections of the cells stained for ZO1 and HA-tagged OCLN.

Figure 13: Rescuing of OCLN-KO clone 1sc3 cells with OCLN mutants.
A) Establishment of OCLN-knockout clone 1sc3 cells. OCLN-knockout cells were generated from the Huh-7 clone 1sc3 [4,5] by the CRISPR/Cas9 system. OCLN expression in the lysates of parental clone1sc3 cells (Ctrl), OCLN-KO clone 1sc3 cells (OCLN-KO), OKH4 and Huh-7.5 cells were analyzed by Western blotting using anti-OCLN mAb.
B) Cell surface expression of OCLN mutants in complemented OCLN-KO clone1sc3 cells. OCLN-KO clone 1sc3 cells were transduced with lentiviral expression vectors for wild-type (wt) and mutant OCLN. At 48h post-transduction, the cells were biotinylated at 4°C or let untreated (Ctrl) and subsequently lysed. Cell surface biotinylated proteins present in the lysates were pulled down with streptavidin agarose beads. OCLN abundance was determined by Western blot analysis using an anti-HA mAb (Biotinylated). The total amount of HA-OCLN present in the lysate was determined by Western blotting using an anti-HA mAb (Total).
C to E) Intracellular localization of OCLN mutants in complemented OCLN-KO clone1sc3 cells. C) OCLN-KO clone 1sc3 cells were transduced with lentiviral expression vectors for wt and mutants OCLN constructs or not (Ctrl). At 48h post-transduction, cells were fixed with PFA and processed for double label staining of HA-tagged OCLN and ZO1. D) OCLN-KO clone 1sc3 cells were co-transduced with lentiviral expression vectors for wt OCLN, OCLN-C15 or OCLN-C18 and with lentiviral expression vectors for CD81-GFP or CLDN1-Cer. The cells were fixed and

stained for HA-tagged OCLN. Z stacks of xy sections of the cells were acquired by confocal microscopy and 3 different z sections are presented. Bars, 10 μm. E) y-z projection of the cells stained for HA-tagged OCLN and expressing CD81-GFP or CLDN1-Cer are shown. CD81-GFP, CLDN1-Cer are depicted in green, HA-tagged OCLN in red, and nuclei in blue.

Figure 14: Ability of OCLN mutants to mediate HCV infection in complemented OCLN-KO clone 1sc3 cells. OCLN knockout clone 1sc3 cells were transduced with lentiviral expression vectors for the different HA-tagged OCLN mutants and wt OCLN. At 48h post-transduction, expression levels of the mutants in the transduced cells were analyzed by Western blotting using an anti-HA monoclonal antibody (A). In parallel, transduced cells were infected with HCVcc. At 30h post-infection, infectivity levels were determined via immunofluorescence using the A4 anti-E1 mAb. Infectivity is expressed as the percentage of the infection level obtained in OCLN-KO 1sc3 cells complemented with wild-type OCLN (B). Mean values and standard deviations from at least three independent experiments are shown. *P<0.05 in the Wilcoxon signed-rank test.

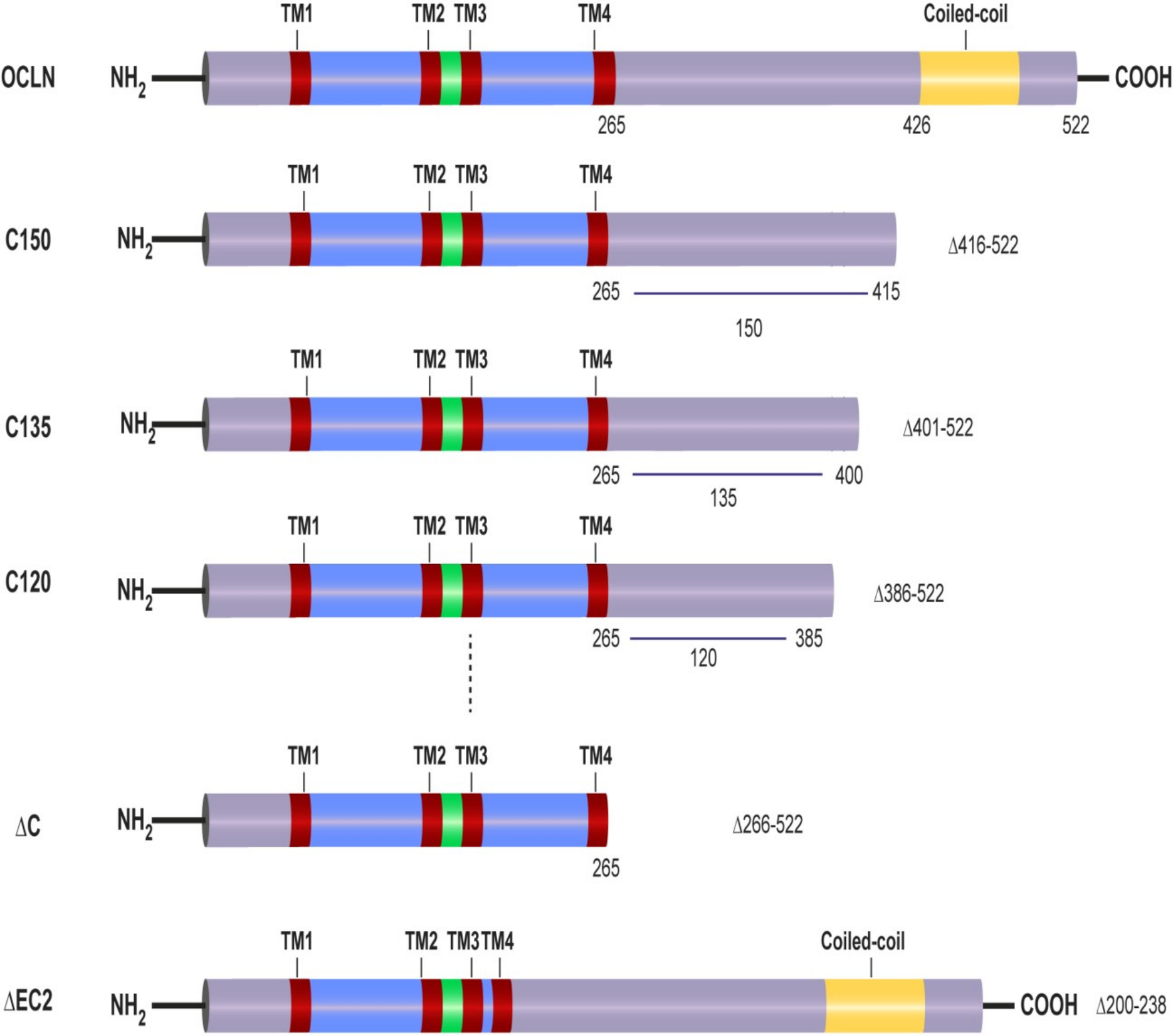
OCLN
NH2
TM1
TM2 TM3
TM4
Coiled-coil
COOH
265
426
522
C150
Δ416-522
415
150
C135
Δ401-522
400
135
C120
Δ386-522
385
120
ΔC
Δ266-522
ΔEC2
TM2 TM3TM4
Δ200-238

Figure 1

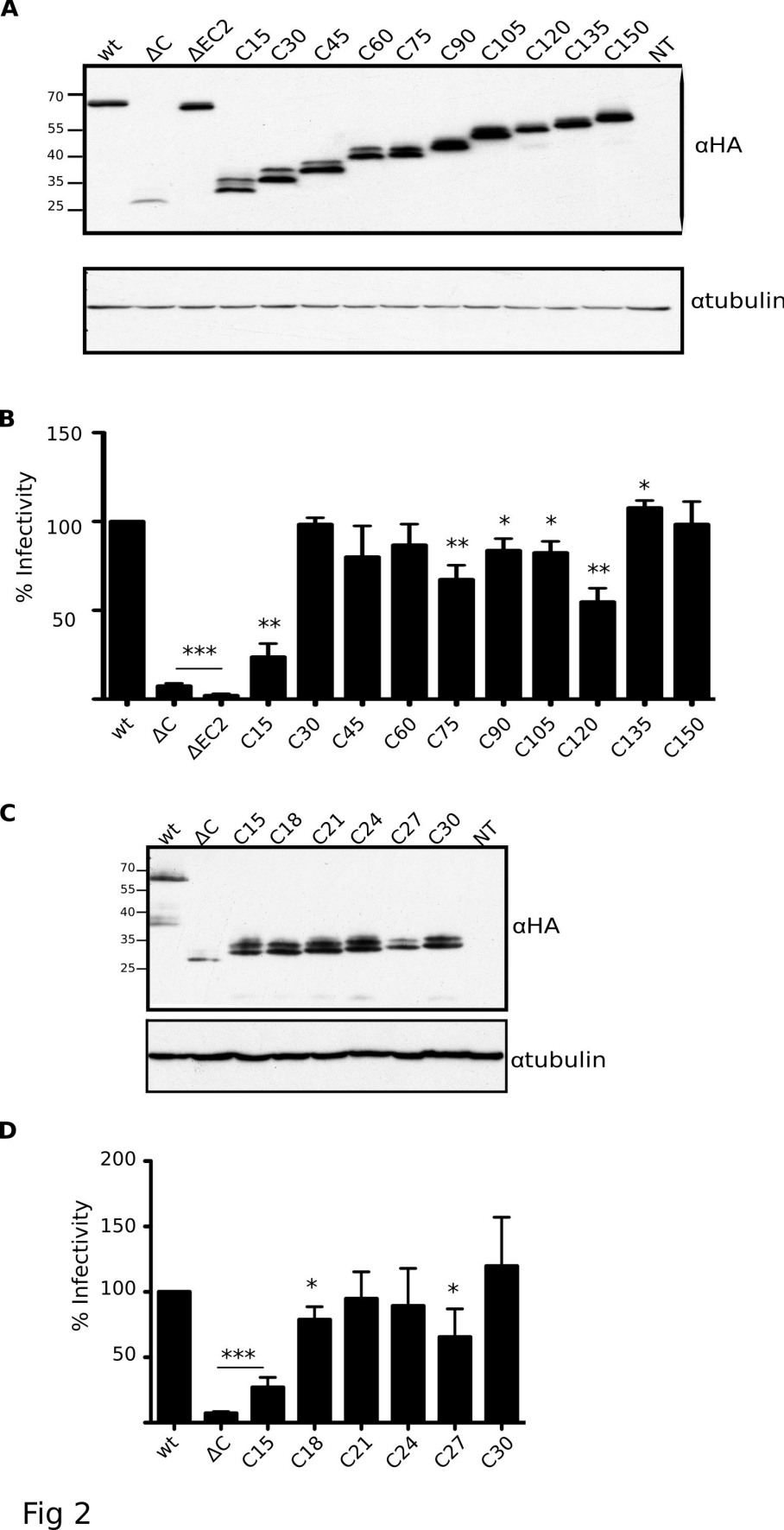
A
wt
ΔC
ΔEC2
C15
C30
C45
C60
C75
C90
C105
C120
C135
C150
NT
70
55
40
35
25
αHA
αtubulin
B
% Infectivity
150
100
50
***
**
*
wt
ΔC
ΔEC2
C15
C30
C45
C60
C75
C90
C105
C120
C135
C150
C
wt
ΔC
C15
C18
C21
C24
C27
C30
NT
70
55
40
35
25
αHA
αtubulin
D
% Infectivity
200
150
100
50
***
*
wt
ΔC
C15
C18
C21
C24
C27
C30

Fig 2

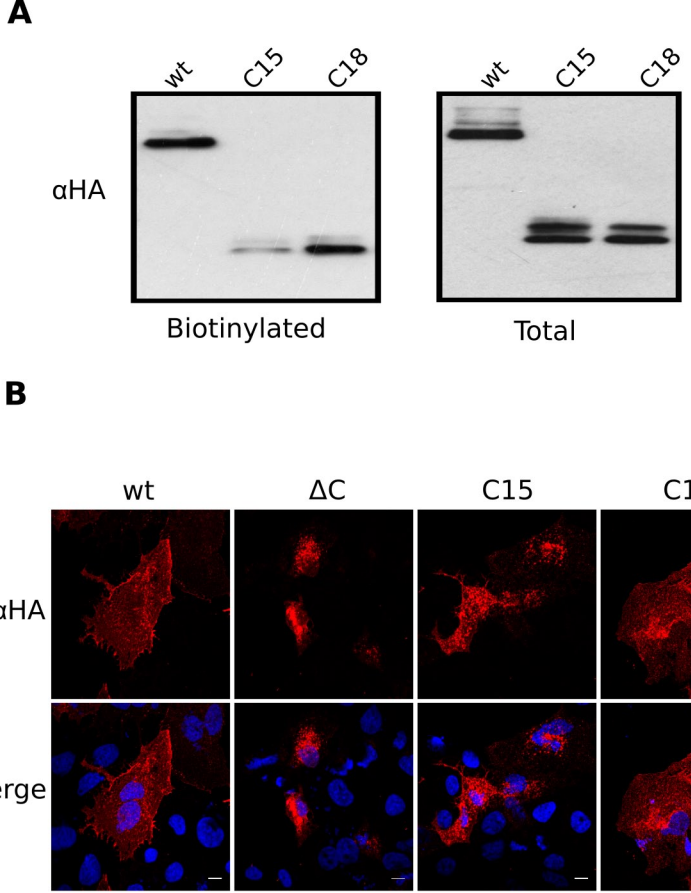
A
wt
C15
C18
αHA
Biotinylated
wt
C15
C18
Total
B
wt
ΔC
C15
C18
αHA
Merge

Fig 3

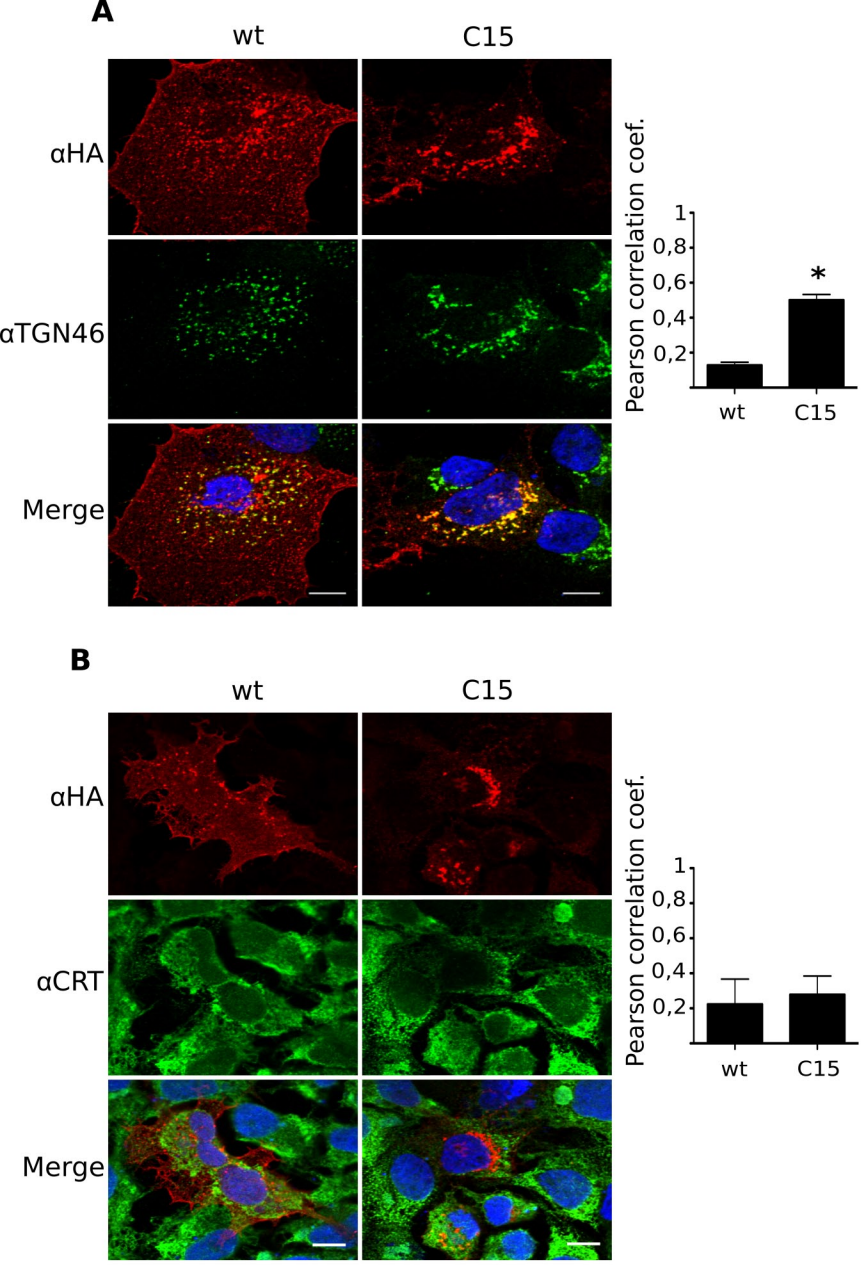
A
wt
C15
αHA
αTGN46
Merge
Pearson correlation coef.
1
0,8
0,6
0,4
0,2
*
wt
C15
B
wt
C15
αHA
αCRT
Merge
Pearson correlation coef.
1
0,8
0,6
0,4
0,2
wt
C15

Fig4

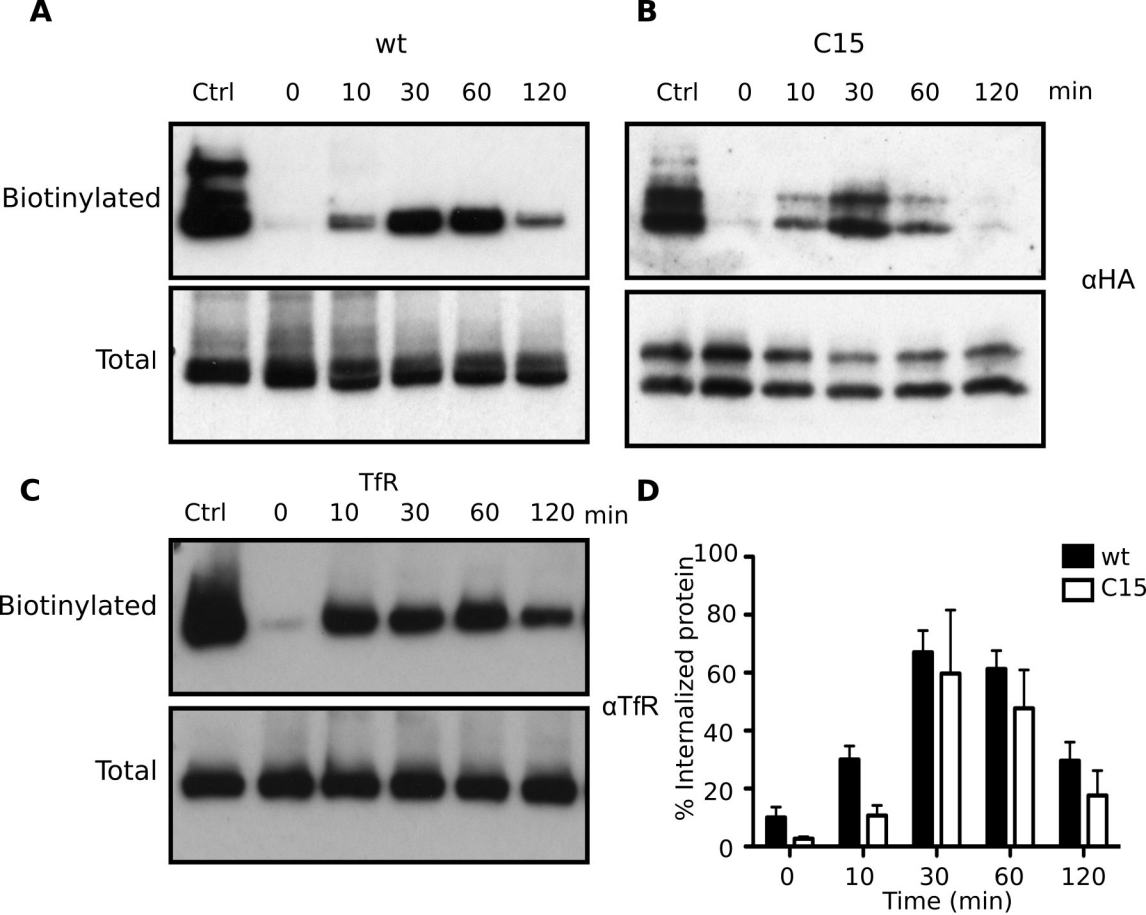
A
wt
Ctrl 0 10 30 60 120
Biotinylated
Total
B
C15
Ctrl 0 10 30 60 120 min
αHA
C
TfR
Ctrl 0 10 30 60 120 min
Biotinylated
Total
αTfR
D
% Internalized protein
100
80
60
40
20
0
wt
C15
0 10 30 60 120
Time (min)

Figure 5

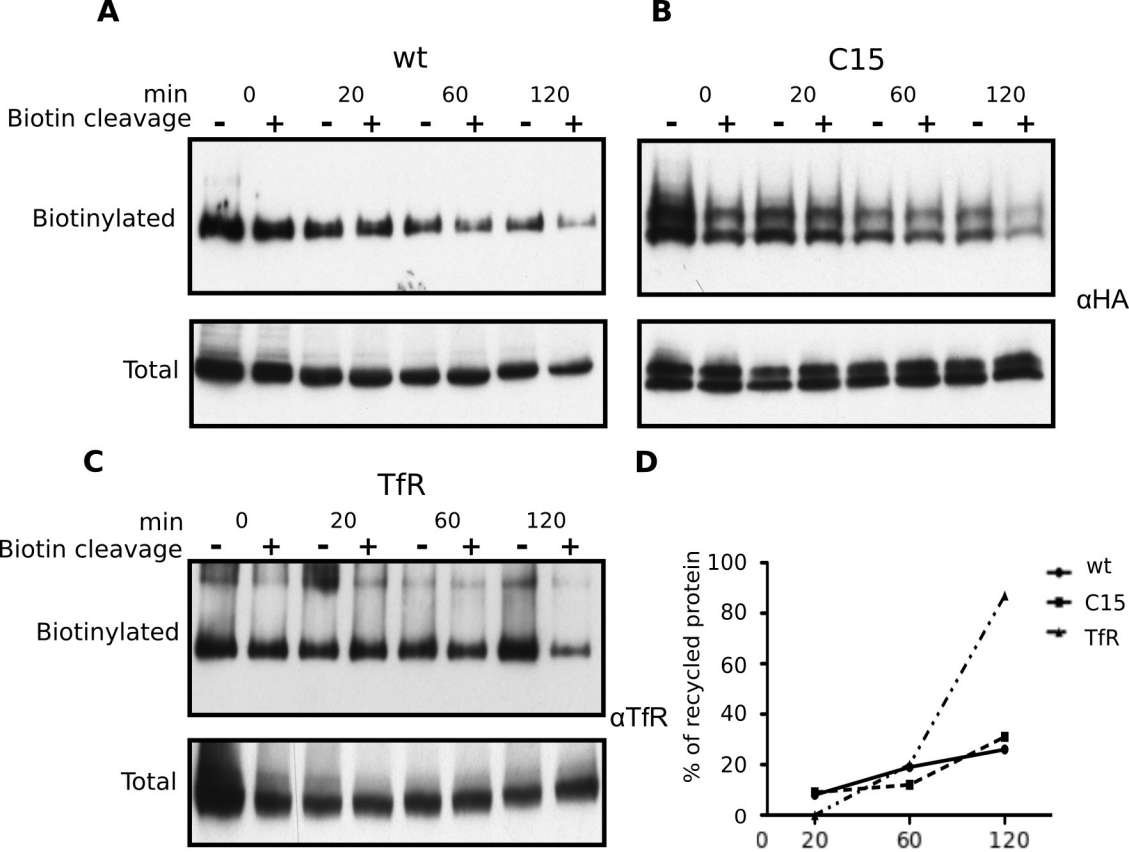
A
wt
min
0
20
60
120
Biotin cleavage
- + - + - + - +
Biotinylated
Total
B
C15
0
20
60
120
- + - + - + - +
αHA
C
TfR
min
0
20
60
120
Biotin cleavage
- + - + - + - +
Biotinylated
αTfR
Total
D
% of recycled protein
100
80
60
40
20
0
0
20
60
120
wt
C15
TfR

Figure 6

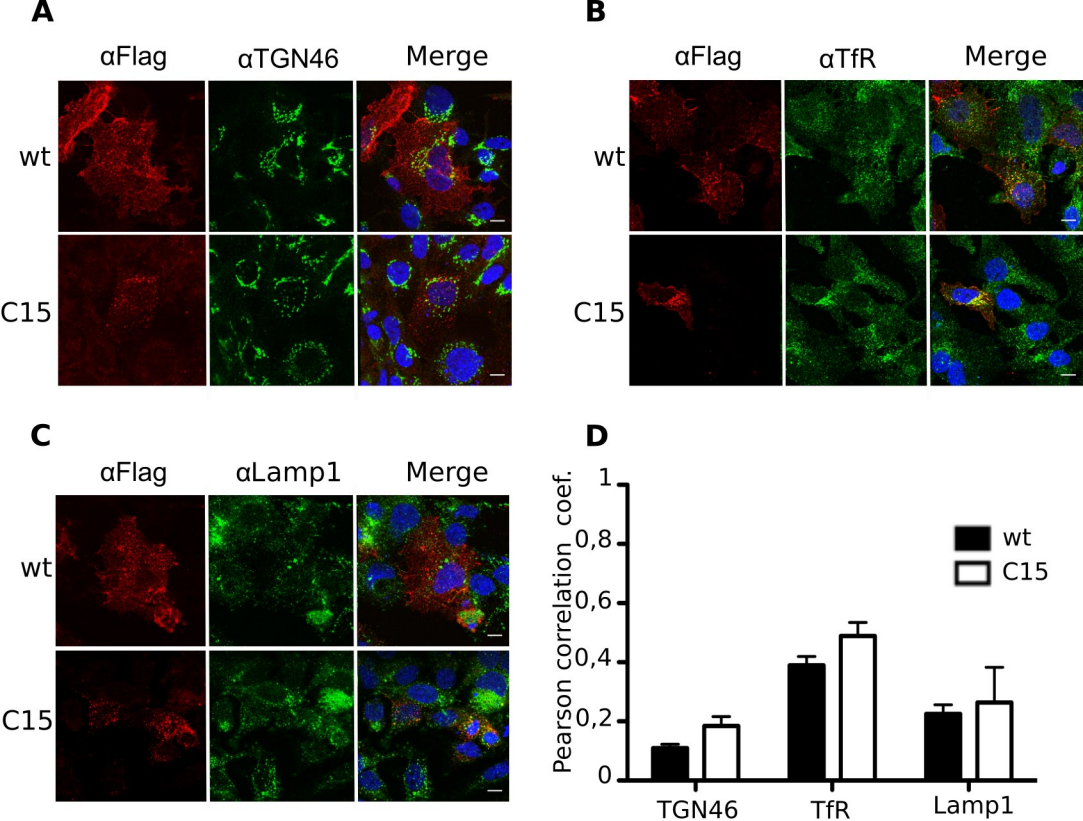
A
αFlag
αTGN46
Merge
wt
C15
B
αFlag
αTfR
Merge
wt
C15
C
αFlag
αLamp1
Merge
wt
C15
D
Pearson correlation coef.
1
0,8
0,6
0,4
0,2
0
wt
C15
TGN46
TfR
Lamp1

Figure 7

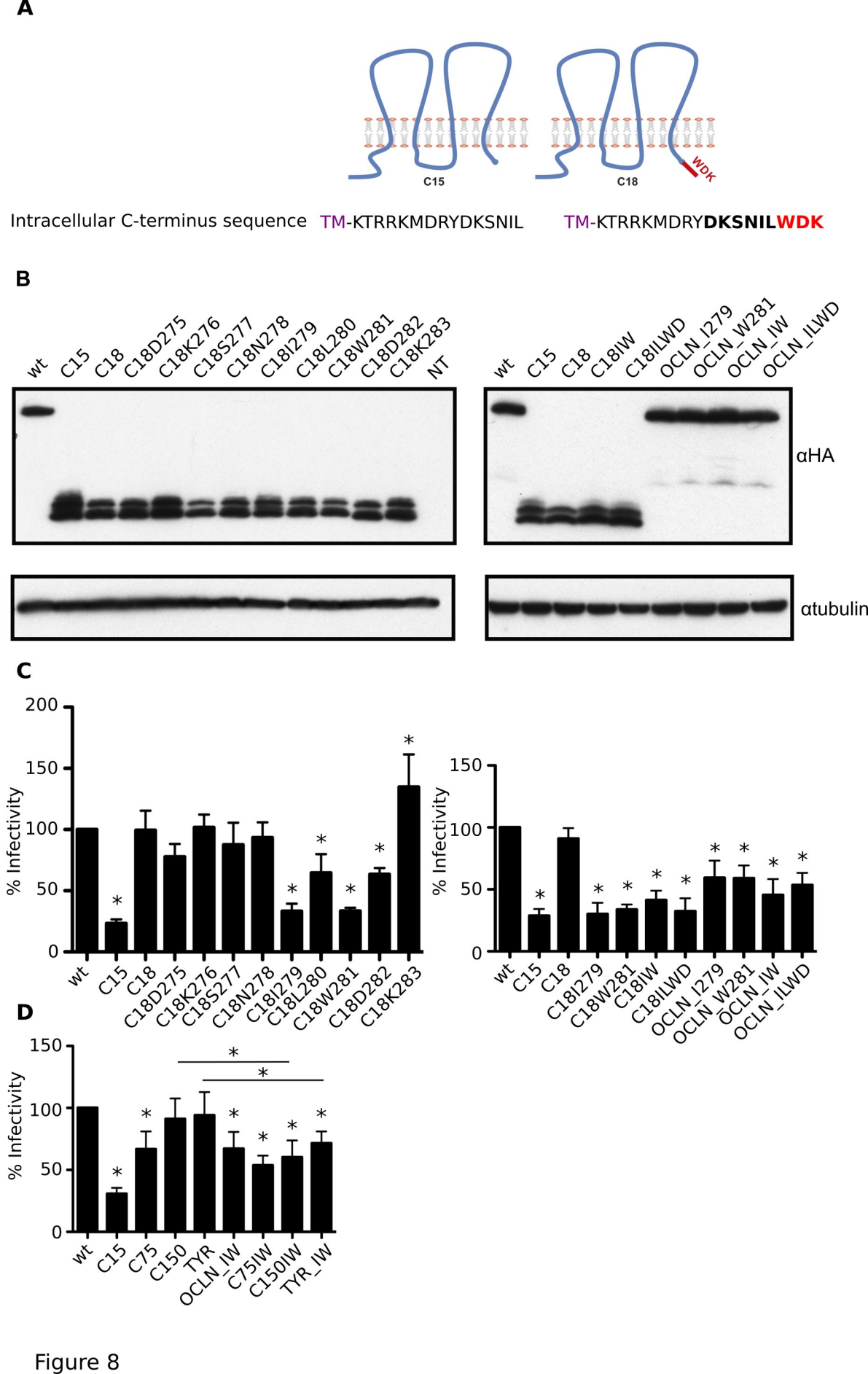
A
C15
C18
WDK
Intracellular C-terminus sequence TM-KTRRKMDRYDKSNIL TM-KTRRKMDRYDKSNILWDK
B
wt C15 C18 C18D275 C18K276 C18S277 C18N278 C18I279 C18L280 C18W281 C18D282 C18K283 NT
wt C15 C18 C18IW C18ILWD OCLN_I279 OCLN_W281 OCLN_IW OCLN_ILWD
αHA
αtubulin
C
% Infectivity
200
150
100
50
0
wt C15 C18 C18D275 C18K276 C18S277 C18N278 C18I279 C18L280 C18W281 C18D282 C18K283
wt C15 C18 C18I279 C18W281 C18IW C18ILWD OCLN_I279 OCLN_W281 OCLN_IW OCLN_ILWD
D
% Infectivity
150
100
50
0
wt C15 C75 C150 TYR OCLN_IW C75IW C150IW TYR_IW

Figure 8

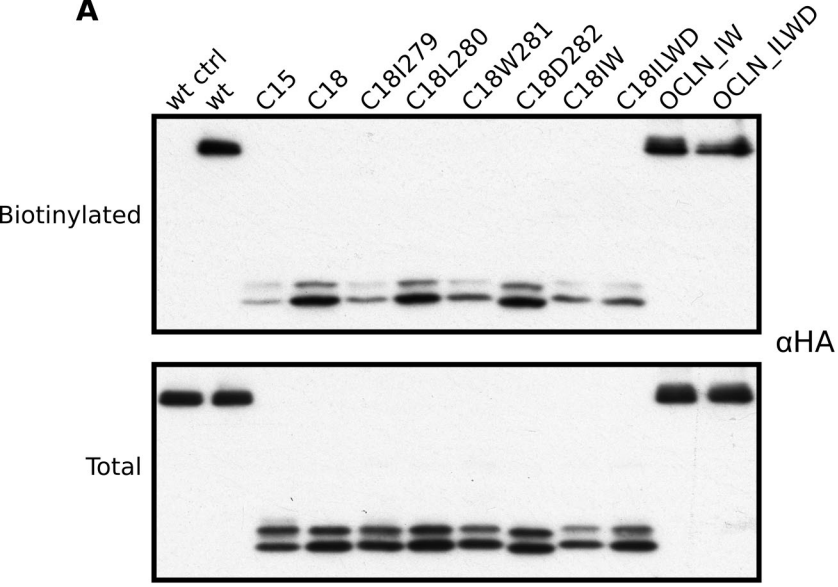
A
wt ctrl
wt
C15
C18
C18I279
C18L280
C18W281
C18D282
C18IW
C18ILWD
OCLN_IW
OCLN_ILWD
Biotinylated
αHA
Total

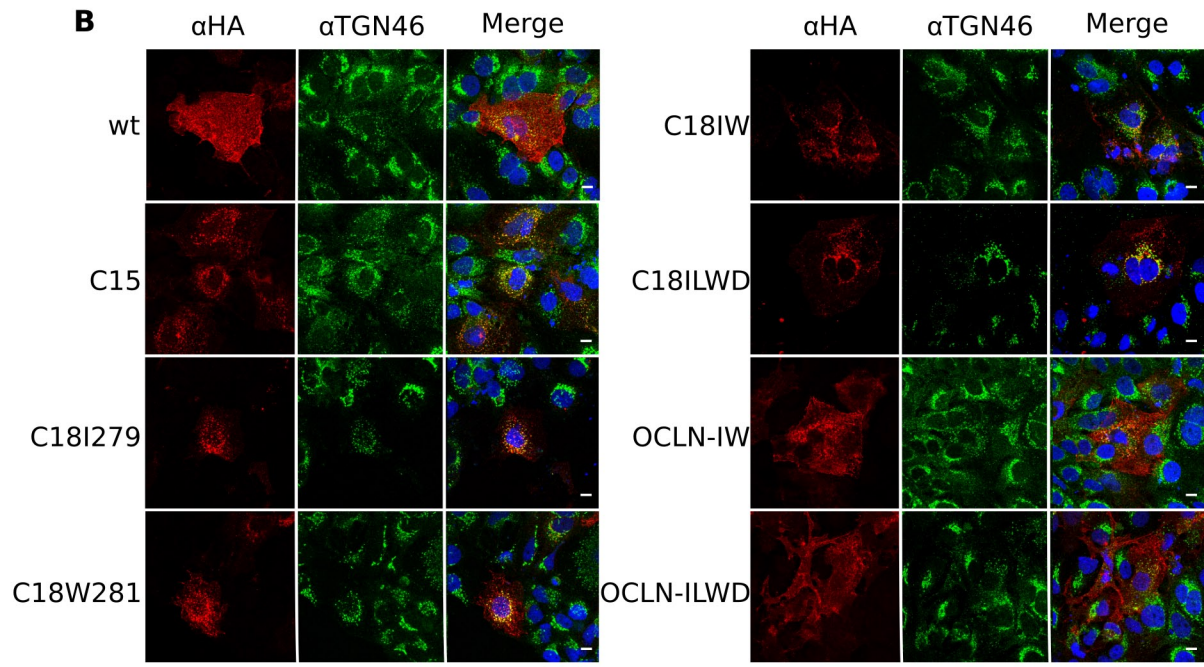
B
αHA
αTGN46
Merge
wt
C15
C18I279
C18W281
C18IW
C18ILWD
OCLN-IW
OCLN-ILWD

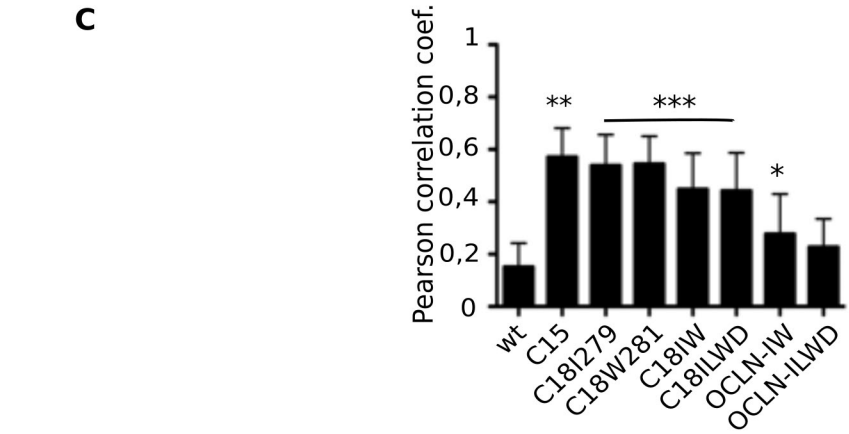
C
Pearson correlation coef.
1
0,8
0,6
0,4
0,2
0
**
***
*
wt
C15
C18I279
C18W281
C18IW
C18ILWD
OCLN-IW
OCLN-ILWD

Figure 9

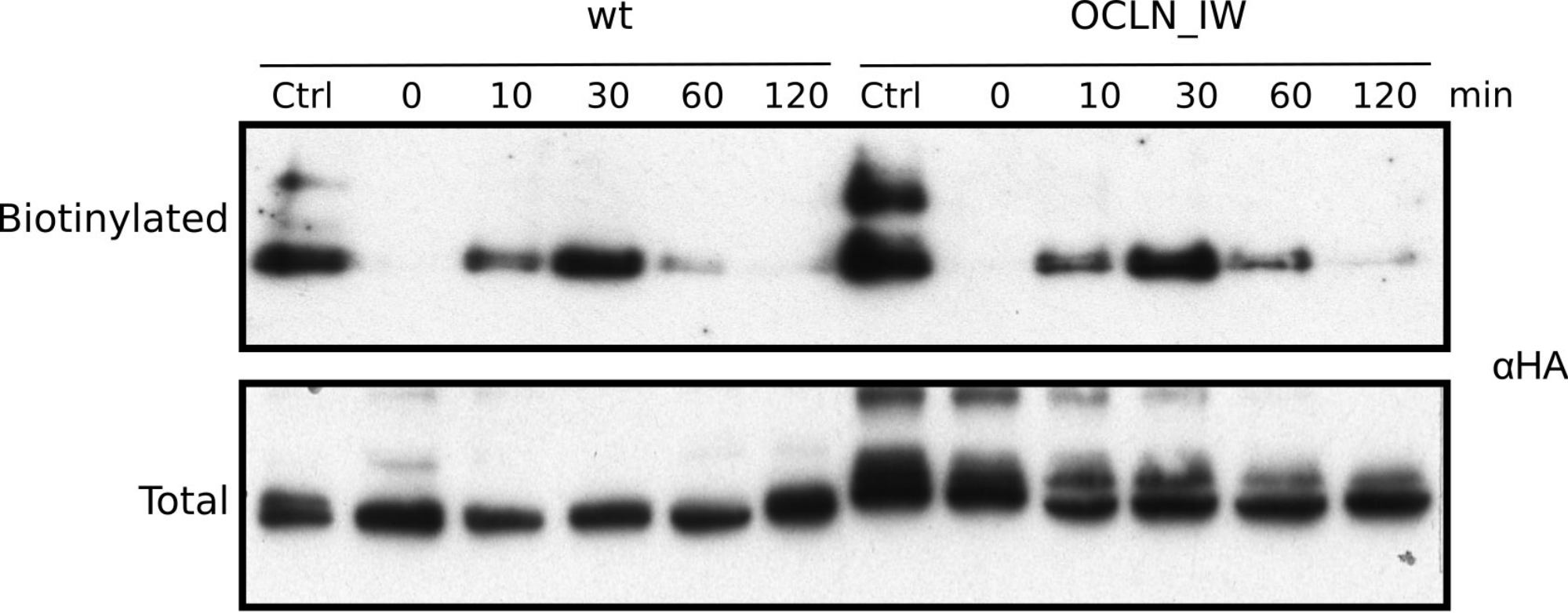
wt
OCLN_IW
Ctrl
0
10
30
60
120
Ctrl
0
10
30
60
120
min
Biotinylated
Total
αHA

Figure 10

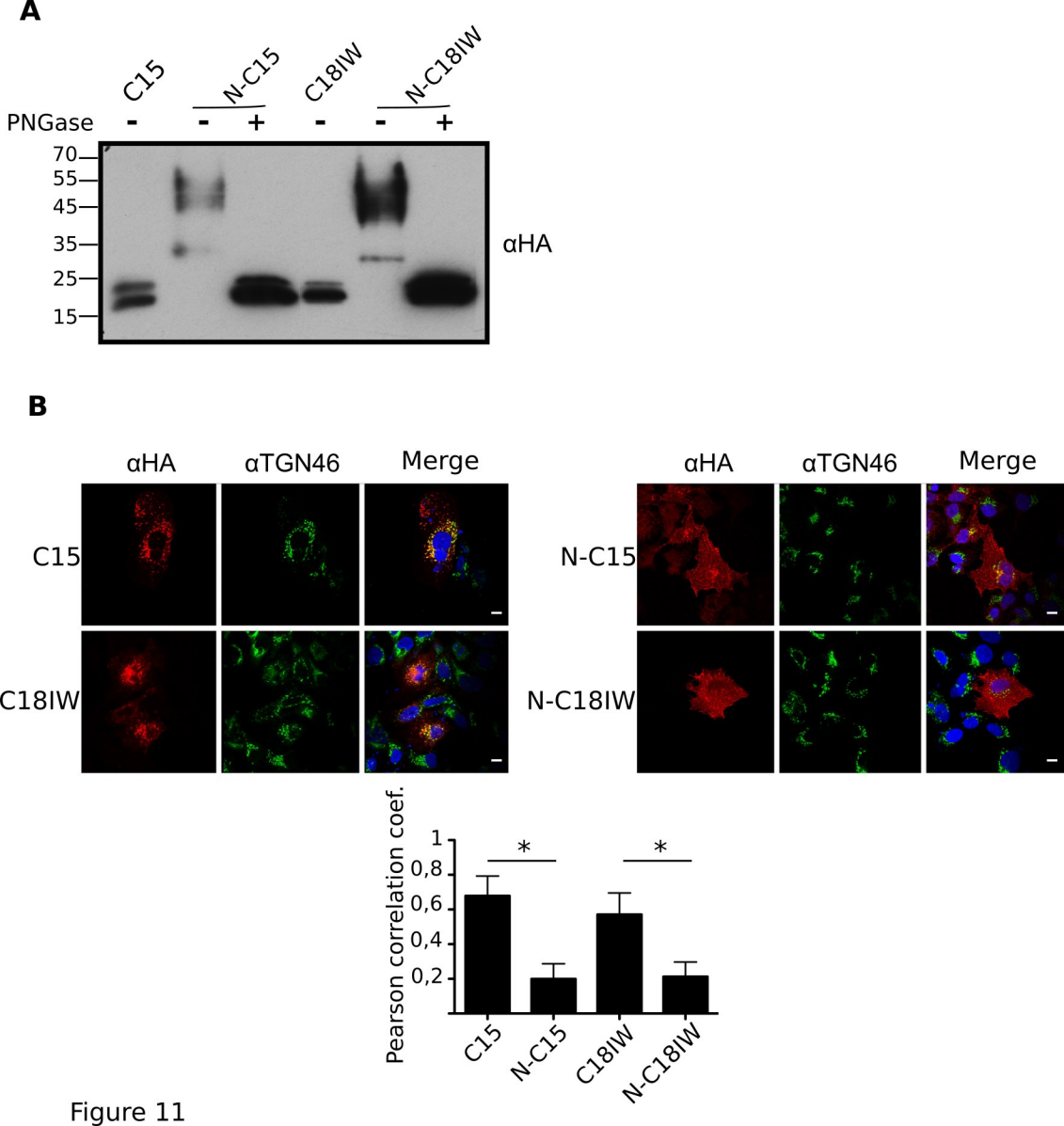
A
C15
N-C15
C18IW
N-C18IW
PNGase
-
-
+
-
-
+
70
55
45
35
25
15
αHA
B
αHA
αTGN46
Merge
C15
C18IW
N-C15
N-C18IW
Pearson correlation coef.
1
0,8
0,6
0,4
0,2
*
*
C15
N-C15
C18IW
N-C18IW

Figure 11

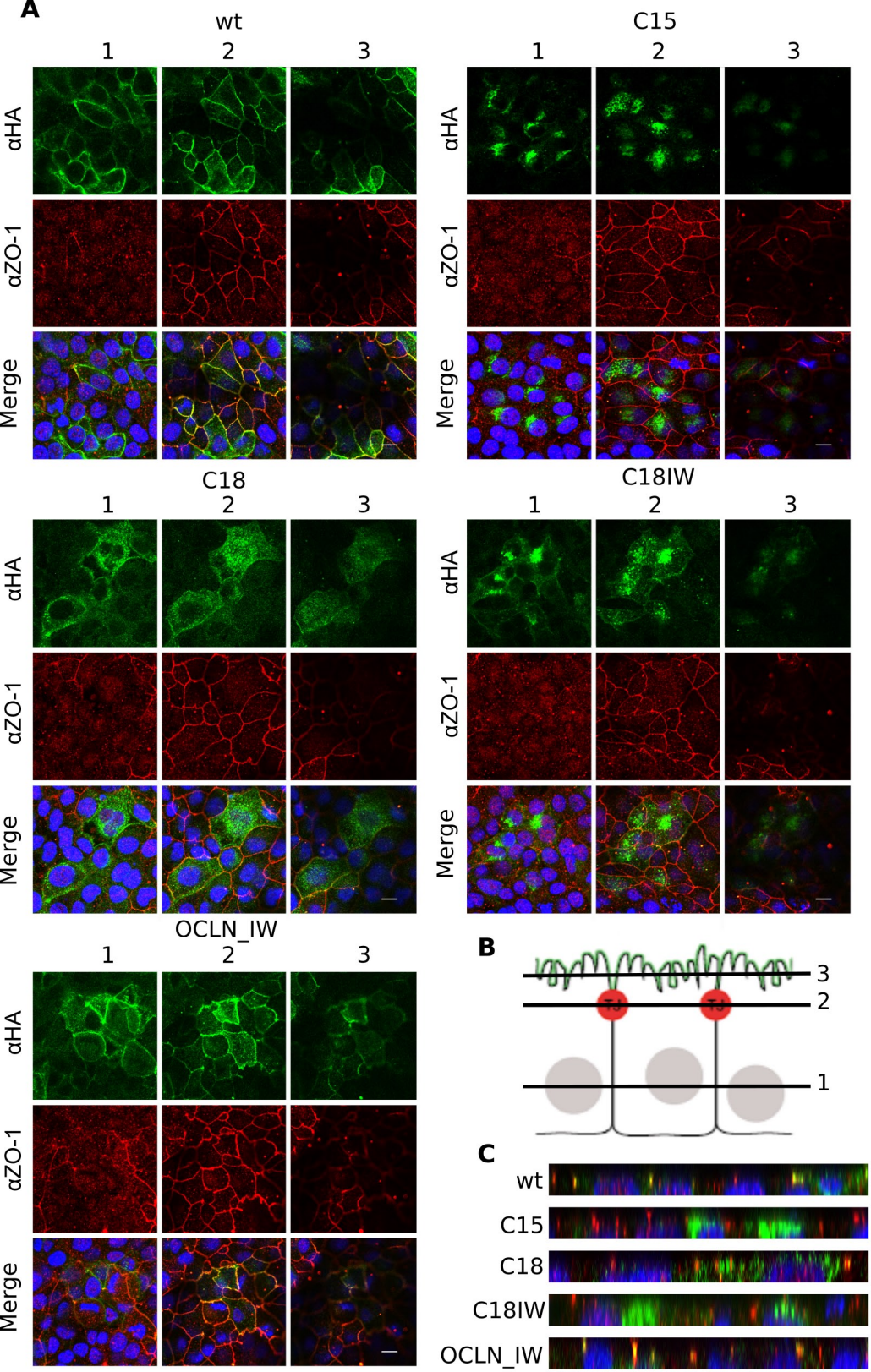
A
wt
C15
C18
C18IW
OCLN_IW
1
2
3
αHA
αZO-1
Merge
B
TJ
TJ
3
2
1
C
wt
C15
C18
C18IW
OCLN_IW

Figure 12

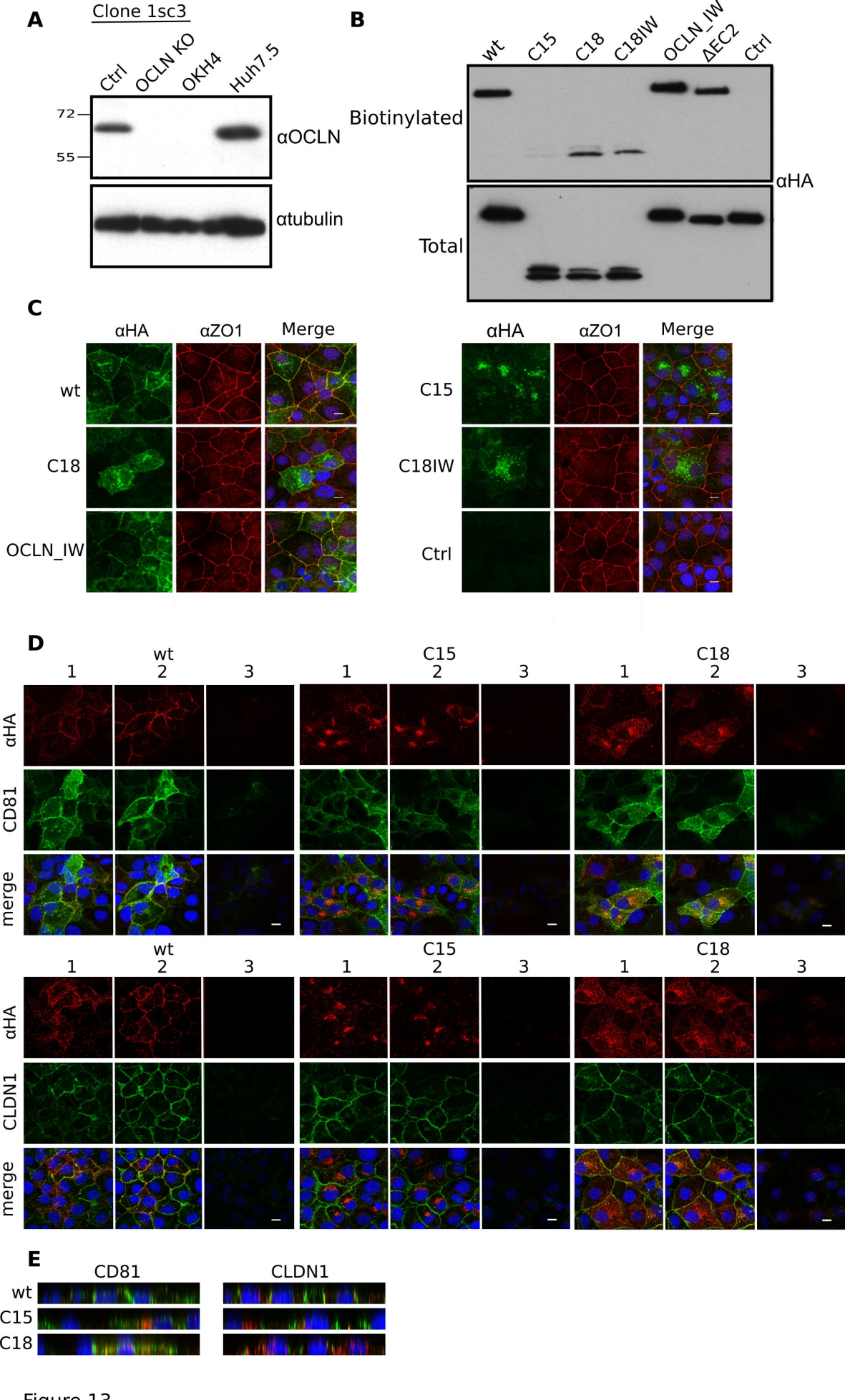
A
Clone 1sc3
Ctrl
OCLN KO
OKH4
Huh7.5
72
55
αOCLN
αtubulin
B
wt
C15
C18
C18IW
OCLN_IW ΔEC2
Ctrl
Biotinylated
Total
αHA
C
αHA
αZO1
Merge
wt
C18
OCLN_IW
C15
C18IW
Ctrl
D
wt
C15
C18
1
2
3
αHA
CD81
merge
CLDN1
E
CD81
CLDN1
wt
C15
C18

Figure 13

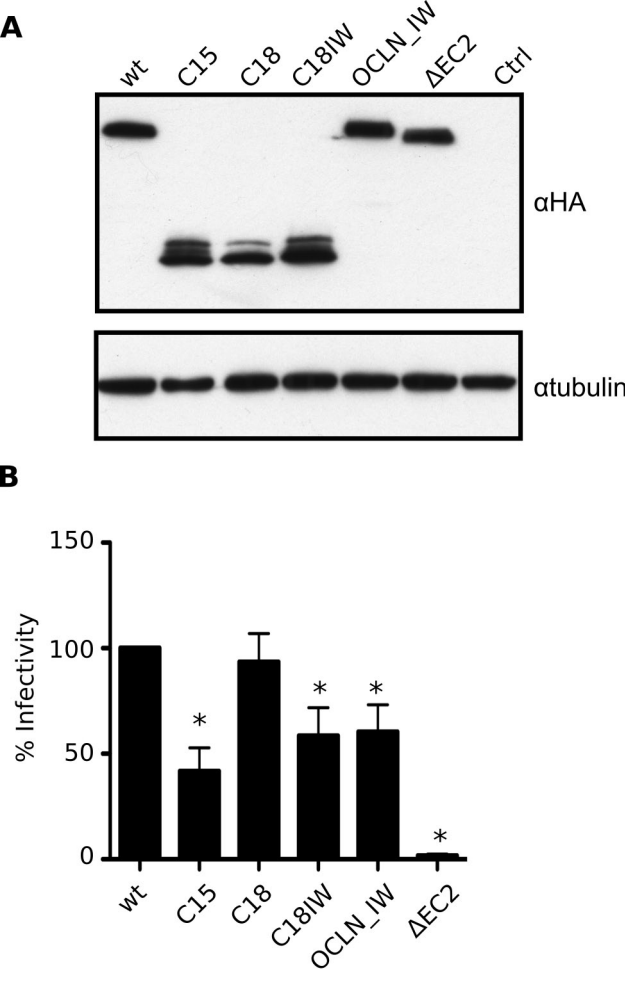
A
wt
C15
C18
C18IW
OCLN_IW
ΔEC2
Ctrl
αHA
αtubulin
B
150
100
50
0
% Infectivity
*
*
*
*
wt
C15
C18
C18IW
OCLN_IW
ΔEC2

Figure 14

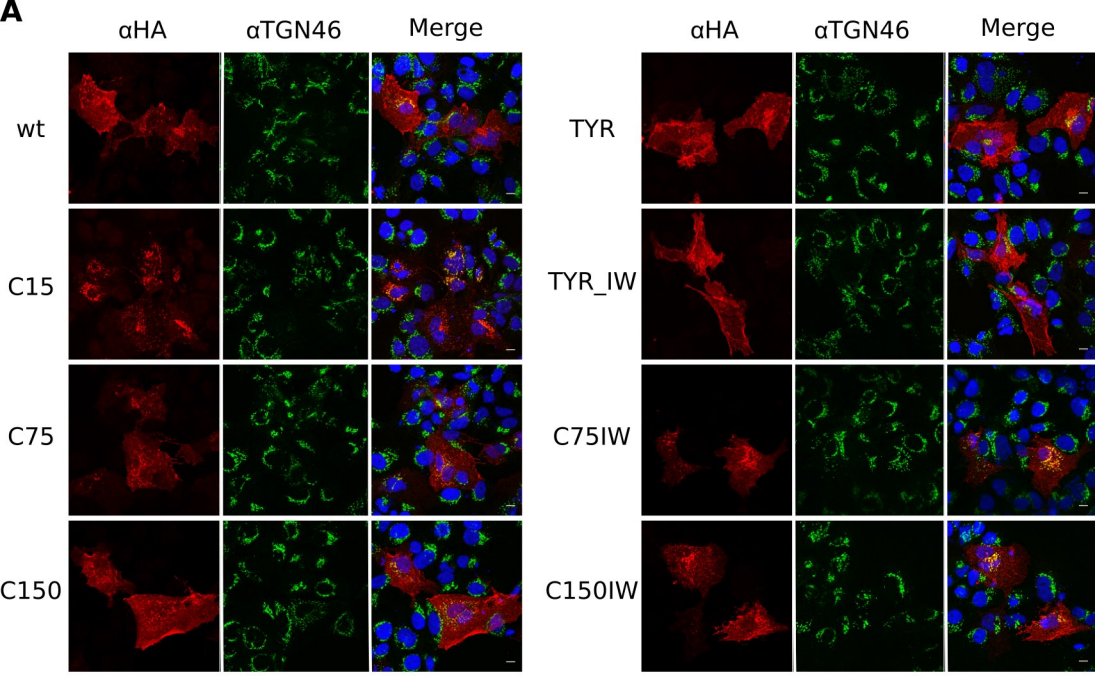
A
αHA
αTGN46
Merge
wt
C15
C75
C150
TYR
TYR_IW
C75IW
C150IW

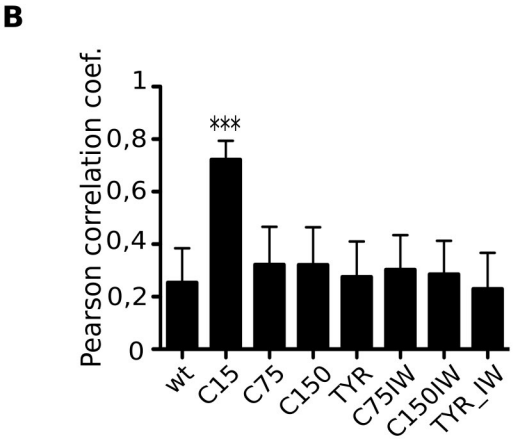
B
Pearson correlation coef.
1
0,8
0,6
0,4
0,2
0
***
wt
C15
C75
C150
TYR
C75IW
C150IW
TYR_IW